



REVIEW ARTICLE

Gasification char residues management: Assessing the characteristics for adsorption application



Anis Atikah Ahmad^{a,b,*}, Mohd Azmier Ahmad^c, Umi Fazara Md Ali^a, Khoo Ken^d

^a Faculty of Chemical Engineering & Technology, Universiti Malaysia Perlis (UniMAP), 02600 Arau, Perlis, Malaysia

^b Centre of Excellence, Water Research and Environmental Sustainability Growth (WAREG), Universiti Malaysia Perlis, 02600 Arau, Perlis, Malaysia

^c School of Chemical Engineering, Engineering Campus, Universiti Sains Malaysia, 14300 Nibong Tebal, Penang, Malaysia

^d Intel Microelectronics (M) Sdn Bhd, Bayan Lepas Free Industrial Zone, Phase 3, Halaman Kampung Jawa, 11900 Penang, Malaysia

Received 22 November 2022; accepted 10 May 2023

Available online 16 May 2023

KEYWORDS

Activated carbon;
Gasification char residues;
Adsorption;
Solid waste

Abstract Due to the world-wide energy crisis and economic issues, biomass has become a resource of global interest as an alternative to activated carbon (AC) produced using non-renewable feedstock (i.e. coal-based). The production of AC from biomass has been determined to be sustainable owing to the abundance of biomass resources on Earth. Biomass gasification has significantly gained market interest and was predicted to reach a value of USD 126 billion by 2023. A critical concern for the existing commercial gasification plants is the handling of char residues, which represent approximately 10% of the initial feedstock mass and are presently treated as waste. The conversion of these chars into AC that can be used for adsorption applications is a possible alternative. This review article focuses on evaluating the characteristic of the gasification char (GC) that is used for adsorption processes. The current AC production method was briefly reviewed. In addition, recent studies on adsorption using GC were explored and summarised.

© 2023 The Author(s). Published by Elsevier B.V. on behalf of King Saud University. This is an open access article under the CC BY-NC-ND license (<http://creativecommons.org/licenses/by-nc-nd/4.0/>).

1. Introduction

Biomass gasification has gained significant attention recently, particularly in developing countries. The IMARC Group esti-

mated that the gasification market reached USD 78 billion in 2017 and anticipated an increasing trend up to USD 126 billion by 2023 (IMARC Group, 2017). Gasification is a thermochemical process where carbonaceous materials are converted into gaseous products at temperatures from 600 to 1000 °C, in the presence of a gasification agent, such as air, oxygen, steam, or a combination of these (Ahmad et al., 2016). The main product of gasification is synthetic gas (usually a mixture of H₂, CH₄, CO, and CO₂), and its composition usually depend on the initial feedstock properties and operational conditions (Ahmad et al., 2016; Al-zareer et al., 2016; Galindo Al et al., 2014), whereby the by-products include char, tar, and

* Corresponding author.

E-mail address: anisatikah@unimap.edu.my (A.A. Ahmad).

Peer review under responsibility of King Saud University.



water vapor. The gasification char (GC) is the irregularly shaped particles which comprised of unreacted carbon with several amounts of siliceous ash. It has well-developed pore properties and potentially become an excellent adsorbent or/and precursor for activated carbon (AC) production. The flow rates of biomass feedstock and gasification agent, equivalence ratio, reactor temperature, and pressure are among the important operating parameters that critically affect the process.

One of the challenges in biomass gasification industry is the solid waste disposal mostly in the form of char, which represents approximately 5–10% of the initial feedstock (De Gisi et al., 2016). Presently, char is treated as waste, which is considered to be an actual loss for plant owners (Benedetti et al., 2017) and no special disposal method has been employed. The growth of gasification industry will create a substantial increase in solid waste management problem. Hence, it is beneficial to seek an alternative application for GC. From the previous finding, GC has shown a reliable performance as an adsorbent in water and wastewater treatment application. However, the research on the GC application in adsorption is quite limited. Several reported literatures regarding its application in adsorption includes malachite green (MG) (Ahmad et al., 2021; Ahmad et al., 2020; Ahmad et al., 2020), rhodamine B (RhB) (Maneerung et al., 2016); methylene blue (MB) (Ahmad et al., 2023; Pessôa, 2019) & amaranth (AM) (Ravenni et al., 2020); congo red (CR) and crystal violet (CV) (Jung et al., 2019); sulphate (Runtti et al., 2016), phosphate & nitrate (Kilpimaa et al., 2015; Kilpimaa et al., 2014), nickel, iron and copper (Runtti et al., 2014); atenolol (ATN) (Ahmad et al., 2020), acetaminophen (ACE) and caffeine (Galhetas et al., 2014; Galhetas et al., 2014), diclofenac (DCF) (Back et al., 2020), toluene (Bhandari et al., 2014) and chromium (III) removal (Godinho et al., 2017; Dias, 2018).

2. Gasification char (GC)

Char is the unreacted carbonaceous solid residue obtained after the gasification process. The physical and chemical properties of char are significant to determine its potential applications. The sorption performance and pore characteristics of adsorbents depend on their physical and chemical properties.

2.1. GC physicochemical properties

The specific Brunauer–Emmett–Teller surface area (S_{BET}), total pore volume (TPV), and average pore diameter (APD) of char are among the most important factors that influence its adsorption performance. The S_{BET} of char is the ratio of the total pore surface area to the total char particle mass (You, 2017). The pore size determines the accessibility of the active sites and mass transfer limitation. According to the International Union of Pure and Applied Chemistry, micropores, mesopores, and macropores are pores featuring diameters of < 2 , $2\text{--}50$, and > 50 nm, respectively (Maneerung et al., 2016; Pessôa, 2019). Particles presenting different pore sizes can be expected to exhibit different behaviours during adsorption, as the pressure increases. The sorption behaviour in micropores is almost entirely dominated by the interactions between the fluid molecules and pore walls. By contrast, the sorption behaviour in mesopores depends not only on the

fluid-wall attractions, but also on the attractive interactions between fluid molecules, which leads to multilayer adsorption and capillary condensation (Thommes, 2010).

The properties of GC are influenced by the gasification operating parameter such as temperature and biomass equivalence ratio (ER). For instance, increasing the gasification temperature can promote the release of volatiles which subsequently increase the char porosity. However, too high temperatures may cause the break-down of pore walls and the consequent sintering of the material with consequent porosity reduction (Benedetti et al., 2017). Zhai et al. (Zhai, 2017) characterised sawdust char obtained at high gasification temperature in steam atmosphere using a fixed bed reactor and discovered that the carbon conversion rate increased as the reaction temperature, time, and steam flow rate increased. The S_{BET} of sawdust ash increased from 948.84 and 987.61 m^2/g when the temperature reached 800 and 1000 $^{\circ}\text{C}$, respectively. Similar observation was found by Pelaez-samaniego et al. (Pelaez-samaniego et al., 2020) who gasified wood in 0.4×0.102 m (length \times internal diameter) reverse downdraft gasifier. The upsurge trend of char S_{BET} from 379 to 517 m^2/g was reported with increasing temperature from 725 to 838 $^{\circ}\text{C}$. This was due to the release of volatiles and tar at high temperatures (Tian et al., 2020). Besides, a remarkable improvement of pore structure was observed by Zhang et al. (Zhang et al., 2020) with the S_{BET} and TPV prominently increased from 186 to 552 m^2/g and 0.252 to 0.665 cm^3/g , respectively, due to the increase of gasification rate in Boudouard reaction at high temperature. Higher gasification temperature could accelerate the carbon burn-off, leading to the broadening of the existing pores and thus enlarging the surface area or pore volume (Zhang et al., 2018; Zhang et al., 2018). However, at very high temperature (> 1200 $^{\circ}\text{C}$), the excessive consumption of the residual carbon matrix in the char could lead to the collapse of the developed porous structure; the blockage of some pores (due to enrichment of the inherent inorganic elements); and the fusion and sintering of the pores (Zhai, 2017). In general, increasing operating temperature can extremely increase the gasification reaction rate, but at very high temperature, the char surface area and pore volume may not be linearly improved.

Another important parameter in gasification is ER, which is defined as the ratio of the biomass mass flow rate to the air mass flow rate divided by the same ratio at the stoichiometry of the reaction considered (Palies, 2020). The increase in the relative biomass/air ratio resulted in producing more aromatic and stable char, and the increase in carbonisation reaction extent. Qian et al. (Qian, 2013) investigated the effects of biomass (switchgrass, sorghum straw and red cedar) and ER (0.20, 0.25 and 0.28) on the physicochemical properties of GC, and determined that as the ER increased, the ash content and S_{BET} of most char increased, while the moisture and fixed carbon contents of the char decreased. Furthermore, using Fourier transform infrared spectra results, they concluded that the surface functional groups of char were found to differ between biomass types, but remained similar with the change in ER. Meanwhile, Liu et al. (Liu, 2018) reported that the volatile and fixed carbon of the chars decrease with ER rising, leading to the increase in the ash content. This was due to the increase in the ratio of oxygen and fuel with ER rising, resulting in more consumption of fixed carbon in the gas–solid reactions.

Char production was reported to increase from 0.15 kg/kg to 0.18 kg/kg when increasing ER from 1.6 to 4.6 (Hernández et al., 2016). Higher ER values also lead to a decrease in the bulk density of the produced char, which indicates the fuel conversion through the release of volatile matter and the conversion of a fraction of the remaining char via heterogeneous reactions (partial oxidation, steam reforming, and Boudouard reaction). Hernández et al. (Hernández et al., 2016) also reported that the carbon content of the char increases from 40% to 55% wt. when increasing the ER, which confirms the progressive carbonisation of the char. However, they found that all the obtained chars have low S_{BET} ($< 70 \text{ m}^2/\text{g}$), which is not suitable for adsorption application without further activation. In another study, GC from straw gasification was reported to have high S_{BET} of $1027 \text{ m}^2/\text{g}$ (Hansen et al., 2015).

Maneering et al. (Maneering et al., 2016) reported that the char has high surface area after steam activation at $900 \text{ }^\circ\text{C}$, proving that activated GC generally have a higher S_{BET} . They prepared AC from woody biomass gasification for dye adsorption and discovered that the S_{BET} had a significant increment from 172 to $776 \text{ m}^2/\text{g}$, which gave it high dye adsorption capability.

In their study on the rate of biomass gasification, Lundberg et al. (Lundberg et al., 2016) found that the S_{BET} of the GC varied from 469 to $1581 \text{ m}^2/\text{g}$, depending on different boundary conditions. Similarly, Dias et al. (Dias, 2017) compared the characteristics of chars from the gasification and pyrolysis of rice waste streams as potential adsorbent materials. They discovered that GC had S_{BET} ranging from 26.9 to $62.9 \text{ m}^2/\text{g}$, while pyrolysis chars lacked a porous matrix due to their high volatile matter content. The authors suggested that GC had favorable properties for adsorption and could be further developed for this purpose, whereas the pyrolysis chars required additional activation.

The choice of feedstock source can significantly affect the final properties of GC. Wood-based GC tend to have a higher S_{BET} and TPV compared to other feedstocks (Oni et al., 2019). This can be attributed to the reduction of relatively large cell structures in wood to smaller pores during gasification, resulting in an overall increase in S_{BET} (Weber and Quicker, 2018) and consequently, PV. The increase in S_{BET} and TPV may also be related to the loss of micro-molecule organic compounds and volatilization of gases or water during gasification, leading to the creation of voids within the GC matrix (Ippolito, 2020). On the other hand, GC produced from manures/biosolids typically exhibit lower S_{BET} , which is likely due to deformation, structural cracking, or micropore blockage during gasification, along with less distinct porous structures in the feedstock (Ahmad, 2014).

In a nutshell, the GC properties vary among the samples depending on the combination of gasification technology, temperature, gasification agent, ER and initial feedstock (Benedetti et al., 2017). Table 1 summarises the physical characteristics of GCs reported in the literature.

Numerous papers have been published on the characterisation of GCs. From the available data, the chars featuring high S_{BET} and TPV values were gasified at high temperature and steam was used as gasification agent. The S_{BET} and TPV values of GCs ranged from 2 to $1581 \text{ m}^2/\text{g}$ and 0.002 to $0.657 \text{ cm}^3/\text{g}$, respectively, and these values were comparable with those of AC, which exhibited S_{BET} and TPV values ranging from 500 to $2000 \text{ m}^2/\text{g}$ and 0.20 to $0.60 \text{ cm}^3/\text{g}$, respectively (Marsh

and Rodríguez-Reinoso, 2006). Therefore, these chars are suitable to be developed as low-cost adsorbents, as they are more affordable and their production require lower energy amounts than AC (since the production of GCs does not involve a carbonisation step). Moreover, the feedstocks for the production of GCs are abundant and are mainly obtained from biowastes.

Despite exhibiting good physical properties, GC cannot be used as sole indicator of good pollutants removal (Abdelhadi et al., 2017). Seredych et al. (Seredych et al., 2009) studied the removal of dibenzothiophene (DBT) and 4,6-dimethyldibenzothiophene (4,6-DMDBT) from effluents using different types of carbon and reported that, although the adsorption of DBT and 4,6-DMDBT was mainly due to the presence of small micropores in the structure of GC, the acidic groups located in the larger pores of the char additionally attracted the DBT and 4,6-DMDBT molecules via specific interactions. In addition, they suggested that the specific carbons that were required for the removal of DBT and 4,6-DMDBT should present high volumes of pores smaller than 10 \AA coupled with certain numbers of strong acidic groups in the slightly larger pores, which would enhance the specific adsorption/surface reactions and at the same time would not block or limit the accessibility of the small pores. These findings demonstrated that the physical properties of chars are not the only factors that could affect the adsorption process. Therefore, it is important to study the chemical properties of GCs.

The chemical characteristics of GC that are relevant to adsorption applications include the carbon and ash contents, functional groups, aromaticity, and pH. Table 2 summarises the total carbon, ash, and elemental composition of several types of GCs. Char presenting high carbon content (50–90%) is suitable to be transformed into AC, which could be used for adsorption (Danish and Ahmad, 2018).

Data on functional groups provide information on the possible interactions between adsorbents and adsorbates. Carboxylic acids, anhydrides, lactones, lactols, and phenols, are acidic, carbonyl and ether groups are neutral, while quinone, chromene, pyrone, and nitrogen groups are basic (Zhai, 2017; Pelaez-samaniego et al., 2020). For AC (Tian et al., 2020; Zhang et al., 2020) and chars (Langley and Fairbrother, 2007), greater amounts of oxygen-containing surface functional groups (especially carboxyl) result in enhanced sorption capacities for metal ions in controlled aqueous media (Uchimiya et al., 2011).

Ogata et al. (Ogata et al., 2011) reported that the sorption capacity of wheat bran for heavy metals depended on the components of the sorbent (pectin and carboxyl groups). Zhong et al. (Zhong et al., 2018) modified commercial AC using nitric acid oxidation and heat treatment at different temperatures to produce different amounts of oxygen-containing surface functional groups. They determined that the oxygen-containing surface functional groups, especially carboxylic groups, controlled the adsorption of MB and methyl orange by AC. Meanwhile, Ducouso et al. (Ducouso et al., 2015) reported that phenol, ether, and quinone were determined to be the dominant oxygen-containing groups on the surface of wood chip gasification biochar. Stavropoulos (Stavropoulos et al., 2008) reported that the phenol adsorption capacity of AC could be enhanced by increasing the content of functional groups on its surface.

Table 1 Physical characteristics of GC residues.

Feedstock	Type of gasifier	Gasification agent	Temperature (°C)	S _{BET} (m ² /g)	TPV (10 ⁻³ cm ³ /g)	Reference
Switchgrass	Fluidised bed	Air (ER = 0.28)	700–800	21	11.88 ^a	(Qian, 2013)
Sorghum		Air (ER = 0.28)		5.6	2.14 ^a	
Red cedar		Air (ER = 0.25)		61	31.33 ^a	
Wheat straw pellet	Circulating fluidised bed	Steam	750	75	40	(Hansen et al., 2015)
Pine wood	Two stage		1000–1200	1027	580	
Sieved pine wood				426	520	
Dealcoholised marc of grape	Entrained flow	Air Steam	1200 1200	60 35	N/A	(Hernández et al., 2016)
Activated mesquite wood chips	Downdraft fixed-bed	N/A	N/A	776	657	(Maneerung et al., 2016)
Soft wood chips	Bubbling fluidised bed	Steam	850	489	N/A	(Lundberg et al., 2016)
Soft wood pellets				1581		
Sawdust	Fixed bed	Steam-air	800–1000	945– 988	N/A	(Zhai, 2017)
Rice husk and polyethylene mixture	Bubbling fluidised bed	Steam-air	850	27–63	N/A	(Dias, 2017)
Wood chips	Downdraft	Air	~650	352	240	(Benedetti et al., 2017)
Pellets	Rising co-current	Air	~700	128	180	
Wood chips	Downdraft	Air	~650	78	80	
Wood chips	Downdraft	Air	~800	281	130	
Wood chips	Dual-stage	Air	~900	587	300	
Wood chips	Dual-stage	Air	~850	272	150	
Pine wood	N/A	N/A	600–900	N/A	N/A	(Marks et al., 2016)
Switchgrass	Downdraft	N/A	N/A	64	90	(Bhandari et al., 2014)
Switchgrass	Fluidised bed	N/A	N/A	2	20	
Pine wood	Updraft	Air	1000	183	90	(Huggins et al., 2015)
Poplar wood	Fluidised bed	Steam	750	573.8	219	(Ducouso et al., 2015)
Woodchip	Downdraft	Air	725–838	517	288.8	(Pelaez-samaniego et al., 2020)
Coal	N/A	CO ₂	800–950	346.74	262.7	(Liu, 2021)
Miscanthus	N/A	Steam	1000	981.75	566.5	(Tian et al., 2020)
<i>Glyricidia sepium</i> woodchip	Downdraft	Air	N/A	39.52	28.0	(Ahmad et al., 2020)
Woodchip	Downdraft	Air	N/A	257.96	87.5	(Ahmad et al., 2020)
<i>Hevea brasiliensis</i> root	Downdraft	Air	N/A	135.22	80.0	(Ahmad et al., 2021)

ER = Equivalence ratio, ^a = Total micropore volume.

Generally the number of functional groups on the surface of GC is small owing to the significant loss of functional groups, such as hydroxyl, carboxyl, and carbonyl at high gasification temperature (Wiedner et al., 2013). Moreover, the number of functional groups also depends on the feedstock used for producing the char. A higher O/C ratio for a char material could indicate the presence of more functional groups (such as hydroxyl, carboxyl, and carbonyl), which could contribute to a higher cation exchange capacity value (Hansen et al., 2015; Lundberg et al., 2016), owing to the higher negative charge on the surface of the char (Xu et al., 2011). Scholars predicted that electrostatic interactions could occur between the negatively charged char surface and positively charged pollutants (Solpan et al.).

A high degree of carbonisation removes the acidic functional groups of the feedstock, therefore causing the char surface to become basic (Shen et al., 2016). Depending on the feedstock used to produce char, the pH of GC is generally alkaline ($7 < \text{pH} < 12$) (Ippolito, 2020; Ahmad, 2014). The

basicity of char is attributed to the presence of small amounts of oxygen-containing groups on its surface. These groups are responsible for the electrostatic interactions between the positively charged char and negatively charged pollutants. In addition, the presence of alkali and alkaline metals such as K and Ca also lead to the alkaline pH (Saffe et al., 2020).

The degree of aromaticity of GC is generally higher (Abdulrazzaq et al., 2014) at high temperature (Huggins et al., 2015; Ducouso et al., 2015). This indicates that GC presents high chemical stability, therefore making it suitable for soil amendment and adsorption applications.

In conclusion, the characteristics of char such as its porous structure, high S_{BET}, large number of surface functional groups, and mineral content make it suitable as adsorbent for removing pollutants from the environment (Marsh and Rodríguez-Reinoso, 2006; Abdelhadi et al., 2017). The oxygen-rich functional groups, including C=O, C–O, and aromatic groups on the surface of GC could act as strong active sites and promote its adsorption capability (Xue, 2012).

Table 2 Chemical characteristics of GC residues.

Feedstock	Technology	Gasification agent	Temperature (°C)	Carbon (%)	Fixed carbon (%)	Volatile matter (%)	Moisture (%)	Ash (%)	Reference
Switchgrass	Fluidised bed	Air	700–800	43.19	15.01	70.36	9.7	4.62	(Qian, 2013)
Sorghum		(ER = 0.20,		40.68	17.46	68.1	9.39	5.05	
Red cedar		0.25, 0.28)		47.51	15.62	71.79	8.5	4.09	
Sorghum	Downdraft	Air	850	67.9	66.8	12.2	0.8	20.2	(Qian et al., 2015)
Red cedar		(ER = 0.20)		66.4	71.7	22.8	1.0	4.5	
Pine wood	N/A	N/A	600–900	79.34	N/A	8.0	N/A	10.79	(Marks et al., 2016)
Poplar wood	Fluidised bed	Steam	750	77.4	N/A	N/A	6.2	3.6	(Ducousso et al., 2015)
Glyricidia sepium	Downdraft	Air	N/A	59.87	67.23	13.51	9.65	9.63	(Ahmad et al., 2020)
woodchip based									
Woodchip	Downdraft	Air	N/A	58.74	75.88	10.79	8.16	5.17	(Ahmad et al., 2020)
<i>Hevea brasiliensis</i> root	Downdraft	Air	N/A	75.12	77.95	10.44	6.51	5.11	(Ahmad et al., 2021)
Corn stover	Fluidised bed	Steam	850	42.0	41.4	8.4	3.2	47.1	(Cheah et al., 2014)
Oak				76.9	N/A	N/A	0.3	N/A	
Spruce wood chips	Downdraft	Air	800	87.6	N/A	N/A	N/A	N/A	(Ravenni et al., 2020)
Municipal solid wast	Downdraft	Steam + Air	N/A	48.3	23.6	26.0	N/A	50.4	(Jung et al., 2019)
Oil sludge	Furnace	Steam	900	5.61	0.13	12.49	1.05	86.33	(Zhiwei, 2021)
Woodchip	Dual stage	Air	850	91.4	N/A	N/A	N/A	4.2	(Benedetti et al., 2019)
Penicillin mycelial dreg and	Thermogravimetric analyzer	Steam	1000	59.64	N/A	N/A	N/A	29.47	(Yuan, 2021)
<i>Pinus patula</i> woodchip	Downdraft	Air	N/A	75.98	89.51	7.23	2.88	3.26	(Pelaez-samaniego et al., 2020)
Pine sawdust	Fixed-bed	CO ₂	N/A	84.83	79.80	19.68	2.01	0.56	(Zhang et al., 2020)

3. Adsorption

Adsorption is a mass transfer process whereby elements gather at the interface of two different phases, such as gas–solid and liquid–solid (De Gisi et al., 2016; Xue, 2012). The adsorbed substance is called adsorbate, while the substance used to adsorb the adsorbate is called adsorbent. Adsorption can be either a chemical (chemisorption) (Aljeboree et al., 2017) or/and physical (physisorption) process (Toumi, 2018). Generally, for physisorption, the attractive forces between the adsorbate molecules and adsorbent are Van der Waals forces, which are weak in nature and result in reversible adsorption. On the other hand, if the attraction forces are due to chemical bonding, the adsorption process is called chemisorption. Chemisorption is characterized by the formation of strong chemical associations between the molecules or ions of adsorbate and the adsorbent surface, which are generally due to the exchange of electrons between them and thus, chemisorption is generally irreversible. In general, the adsorption process involves both chemical and physical adsorption.

Adsorption has been determined to be superior to other pollutants removal techniques owing to its flexibility and simplicity of design, high efficiency, insensitivity to toxic pollu-

tants, and ease of operation compared to other removal techniques such as membrane separation, ion exchange, coagulation/flocculation, chemical oxidation, electrochemical, photochemical and biodegradation. Table 3 summarizes the advantages and disadvantages of various pollutant removal methods.

In adsorption, the removal efficiency depends on the pore characteristics and the surface functional groups of the adsorbent. This information can be examined from the physical and chemical properties of the adsorbent.

4. Activated carbon

Activated carbon is the generic term used to describe a family of carbonaceous adsorbents exhibiting highly amorphous and extensively developed internal pore structure. Activated carbon has been demonstrated to be an effective adsorbent for a wide variety of pollutants from aqueous or gaseous media. Moreover, AC is widely used owing to its exceptionally high surface area (500–1500 m²/g), well-developed internal microporosity (pore size distribution of < 1–100 nm), and wide spectrum of surface functional groups (carboxyl, carbonyl, hydroxyl, and amine) (Zhai, 2017; Danish and Ahmad,

Table 3 Advantages and disadvantages of various pollutant removal technologies (Zhou et al., 2019).

Technology	Advantages	Disadvantages
Adsorption	High efficiency, offer excellent quality of the treated effluent, simple operation (simple equipment, adaptable to many treatment process)	Ineffective to certain pollutants, issues on the disposal of adsorbent residues (elimination of the adsorbent requires incineration, regeneration or replacement of the material).
Membrane separation	Small space requirement, simple, rapid and efficient even at high concentrations	Investment costs are often too high for small and medium industries, high energy requirements, high maintenance and operation costs.
Ion exchange	Rapid and efficient process	Ineffective for certain target pollutants (disperse dyes, drugs, etc.), performance sensitive to pH of effluent, require regular inspection and unloading and loading of new exchange resins, which are disruptive to operations and mean ongoing operational costs
Coagulation/ Flocculation	Rapid and efficient for insoluble contaminants (pigments, etc.) removal	High sludge production and disposal issues, requires accurate chemical dosing (this may be an unsuitable wastewater treatment method if the inlet water quality fluctuates often)
Advanced oxidation process	High efficiency, rapid	Sludge production, economically unfeasible, high chemical reagents and electricity consumption, formation of by-products
Electrochemical process	High efficiency (more effective and rapid organic matter separation than in traditional coagulation), does not require the addition of chemical reagents	High initial cost of the equipment, high electricity consumption
Photochemical process	No sludge production, rapid	The formation of by-products and power consumption

2018). All these characteristics confer AC the extraordinary capacity to adsorb a great diversity of molecules (Ahmad et al., 2020).

Activated carbon can be prepared by physical and chemical activation. Physical activation consists of two steps. The first step involves carbonisation, whereby the precursor material is pyrolyzed in an inert atmosphere at medium–high temperature (300–800 °C) (Danish and Ahmad, 2018; Rivera-Utrilla et al., 2011). The product resulted after carbonisation is called char. The second step is the activation of char at high temperature (700–1000 °C) in the presence of activating agents, such as CO₂ or steam. Since the reactivity of CO₂ at high temperature is lower than that of steam, the activation process using CO₂ can be easier to control, and therefore, CO₂ is more commonly used as activating agent. Additionally, CO₂ activation favours microporosity formation, while steam activation favours microporosity widening. Therefore, AC prepared using steam exhibits lower micropore volume, but larger meso- and macropore volumes than AC prepared using CO₂ (Pallarés et al., 2018).

For chemical activation, the carbon sample is impregnated with various activation agent (e.g. KOH, ZnCl₂, FeCl₃, H₃PO₄, and H₂SO₄) (Shafeeyan et al., 2010; Sánchez-Polo and Rivera-Utrilla, 2002; Klasson et al., 2009), and subsequently, this mixture is pyrolyzed in a conventional furnace (Ribas, 2014) or microwave oven (Rodrigues et al., 2011). The resulting AC product often possesses a large surface area per unit of volume and multi-channel pores that aid the adsorption process (Ogungbenro et al., 2018). Activation agents facilitate the carbonaceous materials decomposition and enhance the carbon yield (Duan et al., 2017). KOH is widely applied and preferred as compared to other activators due to its major role in the improvement of specific surface

area as well as porosity (produces wide and narrow micropores) (Singh et al., 2019). Liu et al. (Liu et al., 2012) reported that the AC prepared by KOH showed improvement in O-containing functional groups. Meanwhile, Shu et al. (Shu et al., 2013) found that the use of ZnCl₂ required low energy consumption, but its volatility and toxicity posed a negative environmental impact. H₃PO₄ treatment offers low operating cost, but the AC specific surface area is somehow smaller than KOH activation (Rajapaksha, 2016).

AC can also be produced through physicochemical activation which combined physical and chemical activation process. It is conducted when chemical activator is not completely diffused which results in pore clogging. This process involves the sample impregnation with chemical agent followed by heating step with the existence of oxidizing gas at 200–900 °C (Chowdhury et al., 2011). The combination of physical and chemical activation promotes the improvement of the pores textural and chemical characteristics compared to single activation method (physical or chemical activation).

However, at industrial scale, physical activation is preferred, to avoid the use of chemicals, which can reduce both the costs of the process and associated pollution. In addition, it could be concluded that physical activation is more adequate than chemical activation for preparing AC intended for applications that require accurate control of pore size distribution (Prauchner and Rodríguez-Reinoso, 2012). Table 4 summarises the activation agents that have been studied for the synthesis of AC.

Previous studies mostly mentioned KOH, ZnCl₂, FeCl₃, H₃PO₄, and H₂SO₄ as activation agents for chemical activation to improve the textural properties and sorption capability of AC. However, it is worth highlighting that chemical activators such as NH₄NO₃ and FeCl₂ are comparable with conven-

Table 4 Various activation agents for the synthesis of AC.

Feedstock	Activation agent	Application	S _{BET} (m ² /g)	TPV (cm ³ /g)	APD (nm)	Reference
Coffee grounds	H ₃ PO ₄	Methylene blue and Nylosan Red removal	925.00	0.718	> 3	(Reffas, 2010)
Celery residues	H ₂ SO ₄	Congo red removal	24.93	0.041	N/A	(Moheballi et al., 2019)
Banana peels	KOH	Methylene blue and Co ²⁺ removal	1396.60	0.750	N/A	(Yu et al., 2018)
Corn starch	KOH	Pyraclostrobin removal	160.60	0.095	2.37	(Suo, 2019)
Pistachio wood wastes	NH ₄ NO ₃	Hg ²⁺ removal	1448.00	0.901	2.48	(Sajjadi, 2018)
Alga (<i>Ulva lactuca</i>)	KOH	Cu ²⁺ , Cr ³⁺ , Cd ²⁺ , and Pb ²⁺ removal	193.90	0.108	1.113	(Ibrahim et al., 2016)
Plum stones	H ₃ PO ₄	Cd ²⁺ and Pb ²⁺ , Ni ²⁺ , and chlorophenols removal	829.00	0.418	1.008	(Pap et al., 2017)
<i>Glebionis coronaria L.</i>	KOH	Cd ²⁺ and Co ²⁺ removal	174.30	N/A	N/A	(Tounsadi, 2016)
Apricot stones	H ₃ PO ₄	Congo red removal	88.05	0.2641	17.632	(Abbas and Trari, 2015)
Date pits	FeCl ₃	Methylene blue removal	780.06	0.573	N/A	(Theydan and Ahmed, 2012)
Waste tea	H ₃ PO ₄	Methylene blue and phenol removal	1398.00	1.177	N/A	(Gokce and Aktas, 2014)
Tomato stems	FeCl ₂	Congo red removal	971.00	0.576	2.782	(Fu et al., 2017)
Rice straw	KOH	Acetaminophen and ibuprofen removal	1330.50	0.522	N/A	(Nam et al., 2018)
Tara gum	FeCl ₃	Antipyrine removal	1680.00	0.990	N/A	(Bedia et al., 2018)
<i>Caesalpinia ferrea</i> seed pod wastes	ZnCl ₂	Captopril removal	1480.00	0.572	N/A	(Kasperiski, 2018)
Date palm tree fronds	CO ₂	N/A	1094.00	0.438	1.609	(Shoib and Al-swaidan, 2015)
Rubber-seed shells	Steam	N/A	948.00	0.988	3.650	(Sun and Jiang, 2010)
Coffee grounds	KOH-steam	Phenol and methylene blue removal	1865.00	0.960	N/A	(Laksaci et al., 2017)
Crofton weed	CO ₂	N/A	1036.00	0.710	2.750	(Zhao-qiang et al., 2014)
Fish waste	Steam	N/A	N/A	N/A	N/A	(Fadhil et al., 2017)
Pinewood soot	Steam	Phenol and chlorine removal	470.00	1.300	N/A	(Trubetskaya et al., 2019)
Tyre carbon black	Steam		470.00	0.600	N/A	
Beechwood soot	Steam		260.00	0.500	N/A	
Wheat straw soot	Steam		400.00	N/A	N/A	
Macadamia nut shells	Steam	N/A	844.00	0.4852	2.301	(Aworn et al., 2008)
	CO ₂		487.00	0.2522	2.070	
Corn cob	Steam		675.00	0.3590	2.128	
	CO ₂		836.00	0.4258	2.042	
Bagasse bottom ash	Steam		595.00	0.3953	2.679	
	CO ₂		546.00	0.3059	2.434	
Sawdust fly ash	Steam		613.00	0.4926	3.216	
	CO ₂		816.00	0.5469	2.682	
Rice husk fly ash	Steam		74.00	0.0532	2.894	
	CO ₂		39.00	0.0296	3.014	

TPV = Total pore volume, APD = Average pore diameter.

tional activators. Meanwhile, steam and CO₂ are commonly used for physical activation.

Presently, most of the CAC is synthesised from non-renewable precursors such as coke, pitch, and coal-based feedstock (Rashidi and Yusup, 2017). The major concerns when utilising these materials are related to their sustainability and high cost owing to the intensive regeneration and reactivation processes they have to undergo, which could also result in the degradation of their adsorption properties and subsequently affect the economic feasibility of the operation (Gupta et al., 2011). Another important AC precursor is coconut shell charcoal, which possess excellent properties as AC. However, the excessive demand of AC led to its mounting prices (Schaeffer, Jun. 2011), hence, other renewable, low-cost adsor-

bents that could be used on large-scale are needed. An adsorbent is considered “low-cost” if it requires little processing and is abundant in nature, or waste material from another industry, which has lost its economic value (Yagub et al., 2014).

5. Recent studies on adsorption applications

Khasri et al. (Khasri et al., 2018) studied the removal of MB using Pentace species sawdust AC (PSAC). They reported that the optimum activation conditions for PSAC were reached when the radiation power, radiation time, and impregnation ratio were 418 W, 6.4 min, and 0.5, respectively, which resulted in the 27% PSAC yield and 94% MB removal. They also

reported that the S_{BET} , TPV, and APD of PSAC were 914.15 m²/g, 0.52 cm³/g, and 3.19 nm, respectively.

The adsorption of acridine orange (AO) was studied using zinc oxide-almond shell AC powder (Zbair et al., 2018). Similar to the findings reported by Khasri et al. (Khasri et al., 2018), the adsorption of AO followed the pseudo second order kinetic model. The maximum removal of AO (99.43%) was achieved at neutral solution pH, when the concentration, temperature, and stirring time were 80 ppm, 40 °C, and 25 min, respectively. Zbair et al. (Zbair et al., 2018) concluded that the electrostatic interactions, π - π interactions, and hydrogen bonding between AO and Zn²⁺/AC were the main possible phenomena involved in the adsorption mechanism.

Bouaziz et al. (Bouaziz et al., 2017) examined the potential of almond gum as low-cost adsorbent for the removal of MG from aqueous solutions. They studied the effects of the adsorbent dose, pH, contact time, particle size, initial dye concentration, temperature, and agitation on dye removal, and reported that the kinetic behaviour was similar with those observed by Khasri et al. (Khasri et al., 2018) and Zbair et al. (Zbair et al., 2018). Based on the thermodynamic changes in enthalpy, entropy, and free energy, Bouaziz et al. (Bouaziz et al., 2017) concluded that the adsorption of MG on the surface of almond gum was endothermic and occurred spontaneously.

The ability of pomelo peels to remove MB from aqueous solution was enhanced by pre-treating them with ultrasounds at 30, 60, and 90% amplitude (Low and Tan, 2018). It was determined that the pre-treated pomelo peels required shorter time to reach their higher saturation limit of the adsorption capacity than the non-treated ones. The Dubinin-Radushkevich model fitted the adsorption isotherm data very well compared to the Langmuir, Freundlich, and Temkin models.

Ahmed & Hameed (Ahmed and Hameed, 2018) prepared pyrolyzed barley straws char for the adsorption of salicylic acid. They investigated the effects of the initial salicylic acid concentration (50–250 ppm), contact time (0–24 h), initial pH (3–11), and temperature (25–45 °C) on the adsorption performance of char, and reported that the equilibrium data fitted well to the Langmuir isotherm, the maximum salicylic acid uptake of 210.6 mg/g being reached at 45 °C. Moreover, they concluded that the adsorption of salicylic acid by char was spontaneous, endothermic, and occurred through chemisorption.

Wheat straw ash was used to synthesise NaY zeolite for the adsorption of tetracycline using the sol-gel method (Ali et al., 2018). The characteristics and effectiveness of NaY as adsorbent for tetracycline were evaluated, and it was determined that the S_{BET} and TPV of the prepared NaY were 657.4 m²/g and 0.34 cm³/g, respectively. The Langmuir equation was successfully applied to analyse the isotherm data, and revealed the maximum equilibrium uptake of 230.7 mg/g at 50 °C.

Ogata et al. (Ogata et al., 2018) prepared wheat bran (WB) for the adsorption of Mo. They used virgin WB, calcined WB (at 200 to 1000 °C), and HCl treated WB (at HCl concentrations from 0.01 to 6.0 mol/L) and reported that the S_{BET} of the calcined WB was larger than that of virgin WB. However, the amount of Mo adsorbed on the virgin WB was greater than that adsorbed on the WB treated using different concentrations of HCl. They concluded that the Mo adsorption mechanism was related to the three-dimensional protein structure of WB.

Table 5 summarises the findings of recent adsorption studies.

Recent adsorption studies indicated the increasing trend in the utilisation of low-cost materials from agricultural residues as well as new applications of char for adsorbing polluting pharmaceutical compounds. However, the agricultural residue from biomass gasification plants (which is GC), has not been well explored yet.

6. Previous studies on liquid adsorption applications using GC residues

Contrarily to other materials used for adsorption studies, the use of gasification residues is scarcely found in the literature. The literature regarding its application in adsorption is somewhat limited to ion and dye removal. Only few researchers reported the emerging contaminant adsorption utilizing GC as adsorbent or precursor for AC.

6.1. Ion removal

The activated char from pine and spruce gasification have been used for removing nitrate and phosphate ions (Kilpimaa et al., 2015; Kilpimaa et al., 2014). Both physical and chemical activation was conducted using char from a downdraft gasifier. Physical activation by CO₂ at high temperature was found to be the most effective process. The maximum monolayer adsorption capability (q_m) of activated char for phosphate and nitrate removal was 80 and 20.5 mg/g, respectively. Similar type of char (pine & spruce) was used by Runtti et al. (Runtti et al., 2014) who studied the adsorption of iron, copper and nickel ions. They gasified the wood chips at a rate of 50 kg h⁻¹ in a 150 kW downdraft gasifier, operating at 1000 °C. They found that the removal of metal ions by GC with and without chemical activation was 2–5 times greater than commercial AC. The highest maximum experimental sorption capacities ($q_{m,exp}$) for iron, copper and nickel by GC were 20.5, 23.1 and 18.2 mg/g, respectively. They concluded that the GC (with and without chemical activation) could be utilized in wastewater treatment due to their high adsorption efficiency. In another study, Runtti et al. (Runtti et al., 2016) chemically activated GC using ZnCl₂, BaCl₂, CaCl₂, FeCl₂ and FeCl₃, for sulphate removal. They revealed that the removal of sulphate ions using FeCl₃ was notably higher ($q_{m,exp} = 19.55$ mg/g) compared to the unmodified GC residue and commercially available AC ($q_{m,exp} = 7.59$ mg/g). The sorption data exhibited PSO kinetics, while the isotherm analysis indicated that the sorption data can be represented by the bi-Langmuir isotherm model.

Godinho et al. (Godinho et al., 2017) analysed the efficiency of chars obtained from the gasification and co-pyrolysis of rice wastes as adsorbents of Cr³⁺ ion from aqueous solutions, and concluded that GC was very efficient to remove Cr³⁺ ion from aqueous solutions, without requiring further activation. A similar study was conducted by Dias et al. (Dias, 2018), who determined that rice waste chars obtained from steam-oxygen gasification presented higher Cr³⁺ ion removal efficiencies and uptake capacities than CAC. Although the prepared chars in this study were very effective for removing Cr³⁺ from aqueous solutions (by both precipitation and adsorption), the char (80% rice husk w/

Table 5 Recent adsorption studies.

Feedstock	Physical properties	Activation conditions	Application	Adsorption capacity (mg/g)	Kinetics	Isotherm	Reference
Medical waste	S_{BET} : 1379 m ² /g TPV: 0.778 cm ³ /g APD: 2.25 nm	Pyrolyzed in an N ₂ atmosphere at 600 °C, KOH activation IR: 1, calcined at 800 °C	MB and reactive yellow (RY) removal	922.2 (MB) 343.4 (RY)	PSO	Langmuir	(Ullah, 2022)
Peanut shell	S_{BET} : 179.3 m ² /g TPV: 0.08 cm ³ /g APD: 1.7 nm	Carbonization & CO ₂ activation flow rate: 100 mL/min, heating rate: 5 °C/min	Naphthenic acids removal	884	Elovich	Langmuir	(Campos et al., 2022)
Pinecone, white popinac, and sugarcane bagasse biochar	N/A	Pyrolyzed in an N ₂ atmosphere at 550 °C for 4 hr and mixed with FeSO ₄ 7 H ₂ O, and MnSO ₄ H ₂ O at	Cu ²⁺ removal	32.7–43.1	PSO	Langmuir	(Huang et al., 2023)
<i>Butiacapitate</i> residue	S_{BET} : 914.15 m ² /g TPV: 0.52 cm ³ /g APD: 3.19 nm	Treatment with ZnCl ₂ IR: 1 and heating at 105 °C (48 h)	Paracetamol and ketoprofenon removal	134.52	N/A	Monolayer & double layer process model	(Yanan, 2022)
Pentace sawdust	S_{BET} : 914.15 m ² /g TPV: 0.52 cm ³ /g APD: 3.19 nm	Power: 418 W Time: 6.4 min KOH IR: 0.5	MB removal	357.14	PSO	Redlich Peterson	(Khasri et al., 2018)
Zinc oxide-almond shell	S_{BET} : 1391.0 m ² /g TPV: 1.26 cm ³ /g APD: 3.21 nm	Temperature: 300 °C (2 h) then 800 °C (3 h) at 10 °C/min. KOH IR: 5	AO removal	909.1	PSO	Langmuir	(Zbair et al., 2018)
Almond gum	N/A	No activation	MG removal	196.07	PSO	Freundlich	(Bouaziz et al., 2017)
Pomelo peel (ultrasound pre-treated)	N/A	No activation	MB removal	113.14 (q _s) 1883.88 (q _m)	N/A	Dubinin–Radushkevich	(Low and Tan, 2018)
Barley straw	S_{BET} : 435.52 m ² /g TPV: 0.241 cm ³ /g APD: 2.216 nm	No activation	Salicylic acid removal	210.56	PSO	Langmuir	(Ahmed and Hameed, 2018)
Wheat straw ash	S_{BET} : 657.44 m ² /g TPV: 0.341 cm ³ /g	No activation	Tetracycline removal	230.69	PSO	Langmuir	(Ali et al., 2018)
Wheat bran	S_{BET} : 0–260.9 m ² /g	No activation	Mo removal	84.0	PSO	Langmuir	(Ogata et al., 2018)
Carbonised cellulose	N/A	No activation	Diclofenac sodium removal	27.3	PSO	Langmuir	(Feng et al., 2018)
Cashew nuts	S_{BET} : 1871 m ² /g TPV: 1.254 cm ³ /g	Treatment with ZnCl ₂ IR: 1.5 and carbonisation at 400 °C (2 h)	MB removal	456	N/A	Langmuir	(Spagnoli et al., 2017)

(continued on next page)

Table 5 (continued)

Feedstock	Physical properties	Activation conditions	Application	Adsorption capacity (mg/g)	Kinetics	Isotherm	Reference
Pyrolyzed crab shells	S_{BET} : 81.57 m ² /g TPV: 0.0861 cm ³ /g APD: 4.22 nm	No activation (only carbonisation by pyrolysis)	MG and CR removal	12 502 (MG) 20 317 (CR)	PSO (MG) PFO and PSO (CR)	Langmuir	(Dai, 2018)
<i>Prunus dulcis</i> leaves	S_{BET} : 426.346 m ² /g TPV: 0.282 cm ³ /g APD: 2.644 nm	Treatment with NaOH IR: 5 and heating at 50 °C (4 h)	Acid green 25 removal	50.79	PSO	Langmuir	(Jain and Gogate, 2018)
<i>Acacia mearnsii</i> waste	S_{BET} : 4.867 m ² /g	Steam explosion (remove tannins) Acetone + H ₂ SO ₄ (acetosolv treatment)	Crystal violet removal	280	HSDM	Freundlich	(Pereira et al., 2018)
Yerba mate	S_{BET} : 20.74 m ² /g PZC = 4.7	No activation	OII and MB removal	47 (OII) 52 (MB)	PSO	Sips	(Albadarin et al., 2018)
<i>Inula viscosa</i> leaves	N/A	N/A	Zn ²⁺ removal	N/A	PSO	Langmuir	(Rouibah, Jan. 2023)
Olive waste residue	PZC = 6.6	Treatment with KOH (0.2 M)	MB removal	504.9	N/A	Langmuir	(Ferkous, 2022)
Cotton fiber waste	N/A	Treatment with ZnCl ₂ IR: 1 and pyrolyzing at 500 °C (1 h)	CI Reactive Red removal	970.34	PSO	N/A	(Behloul, 2022)

S_{BET} = specific Brunauer–Emmett–Teller surface area, TPV = total pore volume, APD = average pore diameter, PZC = point of zero charge, PSO = pseudo second order, PFO = pseudo first order, and HSDM = Homogeneous solid diffusion model, MB = methylene blue, AO = acridine orange, MG = malachite green, CR = congo red, OII = orange II, IR = impregnation ratio, q_{m} = maximum monolayer adsorption capability, q_{s} = Dubinin–Radushkevich constant related to adsorption capacity.

w + 20% w/w polyethylene, with the solid/liquid ratio of 5 mg/L) only presented better results than CAC for the removal of Cr³⁺ from industrial wastewater when precipitation occurred.

6.2. Dye removal

Another application of GC in adsorption was discussed by Jung et al., (Jung et al., 2019), who studied the removal of CR and CV dye using the GC from municipal solid waste. They reported that adsorption performances were higher for municipal solid gasification waste at lower steam rate (37 kg/h) and higher air supply rate (214 Nm³/h, ER = 0.36), which were 49.7 mg/g and 356 mg/g for CR and CV adsorption respectively, suggesting that higher air supply rate with lower steam rate were effective gasification process conditions.

Meanwhile, Maneerung et al. (Maneerung et al., 2016) investigated the removal of RhB using AC from the gasification of mesquite wood chips in a downdraft fixed-bed gasifier, and reported that the prepared AC exhibited high RhB adsorption capability. This was due to its high S_{BET} (776.5 m²/g) and the abundance of carboxyl and hydroxyl groups on its surface. The study also revealed that the equilibrium data ideally fitted to the Langmuir isotherm, the maximum monolayer adsorption capability of AC being 189.8 mg/g, and concluded that, the utilisation of GC as a precursor of AC lowered the AC production cost, offered a cost effective and environmentally friendly method of recycling

char, and lessened the environmental problems related to its disposal.

The removal of MG dye was also reported using GC from gasified *Hevea brasiliensis* root (Ahmad et al., 2021), gasified *Glyricidia sepium* (Ahmad et al., 2020) and gasified wood chip (Ahmad et al., 2020) in batch and fixed bed column adsorption. All the GCs were physicochemically activated via microwave irradiation technique with the aid of KOH and CO₂ as the activation agent. The adsorption capacity and production cost of gasified *Hevea brasiliensis* root, gasified *Glyricidia sepium* and gasified wood chip were 259.49 mg/g and 0.23 USD/kg; 230.47 mg/g and 0.54 USD/kg; and 226.06 mg/g and 0.23 USD/kg, respectively.

Another application of GC in cationic dye removal was reported by Pessôa et al. (Pessôa, 2019) and Ravenni et al. (Ravenni et al., 2020) using GC derived from açai berry (*Euterpe oleracea* Mart) residues and woodchips, respectively. Pessôa et al. (Pessôa, 2019) discovered that the NaOH-activated GC improved the S_{BET} from 1.94 to 491.90 m²/g which led to the increase of MB adsorption capacity from 33.73 to 93.23 mg/g. The performance of activated GC was also tested in raw textile wastewater, which exhibited a reduction of 84.62% in the effluent Biochemical Oxygen Demand (BOD). Meanwhile, Ravenni et al. (Ravenni et al., 2020) reported slightly lower MB adsorption capacity (25.1 mg/g) than Pessôa et al. (Pessôa, 2019), probably due to no GC activation prior to the adsorption as well as different type of GC feedstock was used. Ravenni et al. (Ravenni et al., 2020) also

concluded that the performance of GC for cationic dye-MB (25.1 mg/g) and anionic dye-AM (25.3 mg/g) adsorption were comparable with commercially available AC (25.4 and 23.5 mg/g for MB and AM, respectively).

6.3. Emerging contaminant removal

Galhetas et al. (Galhetas et al., 2014) used K_2CO_3 to activate pine gasification residue for the adsorption of ACE. In another study, Galhetas et al. (Galhetas et al., 2014) also used the gasification residue of pine and coal for ACE and caffeine adsorption from aqueous solutions. They reported that activated pine produced porous materials that aided the ACE and caffeine adsorption processes, which were ruled by the micropore size distribution of the carbons. They concluded that the surface chemistry seemed to be the determinant factor that controlled the affinity of caffeine towards carbons.

Another use of GC for emerging contaminant removal was reported by Ahmad et al. (Ahmad et al., 2020). In this study, the *Glyricidia sepium* woodchip (GGSWAC) was activated via microwave irradiation techniques with the aid of KOH and CO_2 as the chemical and physical agents for ATN adsorption. The BET surface area increased from 39.52 to 483.07 m^2/g after the activation step. It was found that the ATN adsorption fitted well to n-BET model indicating a multilayer adsorption with the saturation capacity of 121, 143 and 163 mg/g at 30, 45 and 60 °C, respectively. Meanwhile, the kinetic study showed that the ATN adsorption followed Avrami model equation with $R^2 = 0.99$. In addition, the adsorption of ATN onto GGSWAC was endothermic ($\Delta H_{S^\circ} = 234.17$ kJ/mol) in the first layer of adsorption and exothermic in the subsequent layer ($\Delta H_{L^\circ} = -165.62$ kJ/mol). The ATN adsorption was controlled by both diffusion and chemisorption. In continuous operation, the Thomas and Yoon–Nelson models successfully predicted the ATN adsorption with R^2 of 0.9822 and 0.9817, respectively. Table 6 summarises the literature findings on the adsorption applications of GC residue.

7. Adsorption mechanisms

The adsorption process involves intermolecular transfer of adsorbate onto the solid surface of the adsorbent. The physical adsorption is carried out mainly through hydrogen bonding, electrostatic interaction and π - π interaction (Sophia and Lima, 2018). Hydrogen bonding (H-bonding) involves the interaction between a hydrogen atom and an electronegative atom (usually N, F, or O). The former is called the H-bond donor, the latter the H-bond acceptor. Previous study showed that the MG adsorption by gasified *Hevea brasiliensis* root (GHRAC) was assisted by H-bonding between the carboxyl groups or hydroxyl groups (H-bond donors) of the GHRAC and H-bond acceptor in MG; as well as H-bonding between hydroxyl group in MG and carbonyl group (H-bond acceptor) of the GHRAC (Ahmad et al., 2021). Besides, H-bond was also found to aid the adsorption of CV and CR onto gasified municipal solid waste based on the shifts in OH peak wavenumber observed from Fourier transform infrared (FTIR) spectroscopy (Jung et al., 2019).

Electrostatic interaction comprises the attractive or repulsive interactions between charged molecules. The opposite charges such as cations (positive) and anions (negative) will

be attracted to each other while the same charges will repel. The electrostatic attraction or repulsion between particles due to their charge can be measured by zeta potential. The electrostatic interaction is commonly influenced by solution pH and ion strength. The influence of pH can be clarified in terms of point of zero charge (pH_{PZC}) value. For cationic adsorbate, at $pH < pH_{PZC}$, the adsorbent surface becomes predominantly positively charged and tend to repel the cationic adsorbate since the number of the negatively charged groups at the surface of the adsorbent decreased, while the positively charged groups increased. Hence the adsorption of the adsorbate molecules to the surface of the adsorbent will commonly declines as pH below pH_{PZC} . In contrast, the adsorbent surface becomes deprotonated at $pH > pH_{PZC}$ due to availability of large number of negatively charged ions, thus adsorbate cations approach strongly towards the negatively charged sites on the adsorbent surface through electrostatic attraction and result in maximum removal (Banerjee et al., 2016). Electrostatic interaction was reported to aid the adsorption of MB onto açai gasification waste (Pessôa, 2019). This was shown by the increase in MB adsorption at pH greater than pH_{PZC} since there is an increase in electron receptor-donor interaction forces between sorbent and sorbate. Other studies that report this type of interaction includes RhB removal by gasified mesquite wood chips (Maneerung et al., 2016), tetracycline removal by biochars derived from alfalfa and Bermuda grass (Jang and Kan, 2019), ACE and MB adsorption by activated biochar derived from municipal solid wastes (Sumalinog et al., 2018) and cephalixin adsorption by pomegranate peel (Rashtbari et al., 2020).

π - π interaction (also known as π - π electron donor-acceptor interaction) involves the interaction between the π electrons in a carbonaceous adsorbent and the π -electron in the aromatic ring of an adsorbate (Tran et al., 2017). π - π interaction generally exists in an aromatic supramolecular system (Gong, 2019). High aromaticity and hydrophilicity of the adsorbent will promote the formation of π - π interactions, in the presence of π electrons in the adsorbate and reactive oxygen groups in the adsorbent (Jung et al., 2019). The adsorbent and adsorbate will bound together by electron transfer between the electron donor and acceptor (Cheng, 2021). This adsorption mechanism plays a leading role in the adsorption process of many carbonaceous materials on various pollutants such as cationic dye (MG, MB) (Ahmad et al., 2020; Ahmad et al., 2020; Pessôa, 2019), anionic dye (amaranth) (Ravenni et al., 2020), reactive dye (remazol brilliant violet 5r) (Khasri et al., 2021), ATN (Ahmad et al., 2020), 2,4-dinitrophenol (Azari et al., 2021), tetracycline (Li, 2022), sulfamethoxazole and Bisphenol A (Ahsan, 2018). Fig. 1 shows the mechanism of ATN adsorption onto gasified *Glyricidia sepium* which involved H-bonding, electrostatic interaction and π - π interaction.

The chemical adsorption involves a chemical bond (covalent or ionic bond) resulting from the substantial sharing or transfer of electrons between the adsorbent and adsorbate. It requires high energy for regeneration and may not be fully reversible. As the adsorbate molecules are adsorbed on the surface of the adsorbent through valence bonds, they form a monolayer adsorption. The chemisorption energy between the adsorbate molecules and adsorbents can vary significantly depending on the bond strength (Kwon et al., 2011). The adsorption mechanisms of various pollutants onto different feedstock of GC are summarized in Table 7.

Table 6 Adsorption using GC residues.

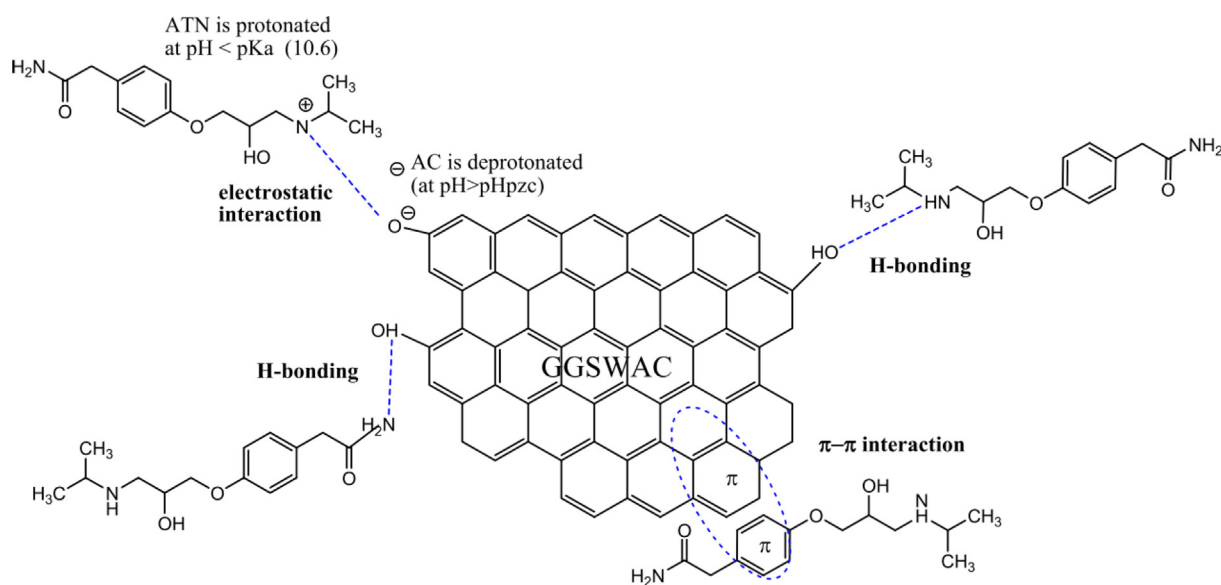
Feedstock	Technology	S_{BET} (m^2/g)	Application	Activation			Adsorption capacity (mg/g)	Remarks	Reference
				Agent	T ($^{\circ}C$)	S_{BET} (m^2/g)			
<i>Hevea brasiliensis</i> root	Downdraft	135.22	MG	KOH- CO ₂	N/A	477.74	259.49	Monolayer and multilayer adsorption involved	(Ahmad et al., 2021)
<i>Glyricidia sepium</i>	Downdraft	39.52	MG	KOH- CO ₂	N/A	633.30	230.47	<i>Glyricidia sepium</i> possessed excellent characteristics for BG4 and ATN removals due to high S_{BET}	(Ahmad et al., 2020)
	Downdraft	39.52	ATN	KOH- CO ₂	N/A	483.07	163		(Ahmad et al., 2020)
Woodchip	Downdraft	257.96	MG	KOH- CO ₂	N/A	351.93	226.06	The optimum activation conditions (radiation power = 616 W, impregnation ratio = 1.06, time = 1 m) resulted in 99.01% MG dye removal	(Ahmad et al., 2020)
Mesquite wood	Downdraft fixed-bed gasifier	776.46	RhB	CO ₂	700	485.20	189.83	prepared AC exhibited high dye adsorption capability	(Maneering et al., 2016)
					800	736.65			
					900	N/A			
				Steam	700	538.98			
					800	736.94			
					900	776.46			
				N ₂	700	177.74			
					800	280.02			
					900	286.90			
Açaí berry seeds	Downdraft	1.94	MB	NaOH		491.90	93.23	Maximum adsorption capacity increased 173% in comparison to non- activated açai biochar.	(Pessôa, 2019)
Woodchip	Downdraft	598	MB	–	–	–	25.1	GC showed a comparable removal efficiency with CAC	(Ravenni et al., 2020)
			AM	–	–	–	25.3		
Municipal Solid waste	Downdraft (low steam rate)	11.4	CR CV	–	–	–	49.7 356	Higher air supply rate with lower steam rate were effective gasification process conditions for CR and CV adsorption	(Jung et al., 2019)
	Downdraft (high steam rate)	2.73	CR CV	–	–	–	35.7 235		
Pine and spruce	150 kW air- blown downdraft gasifier (T = 1000 $^{\circ}C$)	52.4	SO ₄ ²⁻	ZnCl ₂	500			FeCl ₃ -modified carbon residue is a potential sorbent for SO ₄ ²⁻ ion removal which removed SO ₄ ²⁻ ions better than CAC in the concentration range of 50 to 1000 mg/L	(Runtti et al., 2016)
				BaCl ₂	500				
				CaCl ₂	500				
				FeCl ₃	500	52.4	19.5		
				FeCl ₂	500				
Pine and spruce	150 kW air- blown downdraft gasifier (T = 1000 $^{\circ}C$)	52.4	PO ₄ ³⁻ and NO ₃ ⁻	CO ₂	600–	152–	20.5	The sorption capacity can be improved by chemical activation	(Kilpimaa et al., 2015; Kilpimaa et al., 2014)
				CO	800	590	(PO ₄ ³⁻)		
				N ₂	600–	126–	80		
				ZnCl ₂	800	135	(NO ₃ ⁻)		
				HCl	600–	145–			
				H ₂ SO ₄	800	160			
				KOH	N/A	285			
				HNO ₃	N/A	194			
					N/A	157			
					N/A	117			
					N/A	259			

Table 6 (continued)

Feedstock	Technology	S_{BET} (m^2/g)	Application	Activation			Adsorption capacity (mg/g)	Remarks	Reference
				Agent	T ($^{\circ}\text{C}$)	S_{BET} (m^2/g)			
Pine and spruce	150 kW downdraft gasifier (T = 1000 $^{\circ}\text{C}$)	14.4	Ni^{2+} , Fe^{2+} , and Cu^{2+}	ZnCl_2	N/A	259	18.2 (Ni^{2+}) 20.5 (Fe^{2+}) 23.1 (Cu^{2+})	The amounts of pollutants removed by carbon residue with and without activation were higher than those removed by CAC.	(Runtti et al., 2014)
Pine	Fluidised bed reactor (gasification agent = air, T = 850 $^{\circ}\text{C}$)	101	Acetaminophen and caffeine	K_2CO_3	700 800	570 1509	434.8 (ACE) 476.2 (Caffeine)	The increase in temperature resulted in an increase in the sorption capacity	(Galhetas et al., 2014; Galhetas et al., 2014)
Spruce woodchip RH (GC)	Floating-fixed-bed	308.15	DCF	–	–	–	35.09	–	(Back et al., 2020)
RH + PE (PC)	Steam gasification and co-pyrolysis	N/A	Cr^{3+}	N/A	N/A	N/A	21.1 (GC) 1.44 (PC)	GC is better adsorbent than PC. 100% removal GC presented the highest uptake capacity	(Godinho et al., 2017)
50% w/w RH + 50% w/w RS	Bubbling fluidised bed reactor using steam–air as gasification agent	25	Cr^{3+}	N/A	N/A	N/A	8.51	Sorption capacity of GC significantly higher than CAC.	(Dias, 2018)
80% RH w/w + 20% w/w PE	gasification agent	< 5					6.2	The high mineral content of chars played an important role	

S_{BET} = specific Brunauer–Emmett–Teller surface area, RhB = rhodamine B, GC = gasification char, PC = pyrolysis char, AC = activated carbon, CAC = commercial activated carbon, RH = rice husk, RS = rice straw, PE = polyethylene, ID = internal diameter, L = length, L/S = liquid/solid ratio, S/L = solid/liquid ratio, AM = amaranth dye, CR = congo red dye, CV = crystal violet dye, ATN = atenolol, ACE = acetaminophen, DCF = diclofenac, MB = methylene blue dye, MG = malachite green dye.

Summary: Publications on adsorption using GC residue are rather scarce. Based on the limited literature consulted, the adsorption performance of GC residue was demonstrated to be comparable with that of CAC. The sorption process can be further enhanced by various activation processes that could improve the porosity and surface area of char.

**Fig. 1** Mechanism of ATN adsorption onto gasified *Glyricidia sepium* (Ahmad et al., 2020).

8. Factor affecting adsorption

8.1. Effect of initial concentration and contact time

The adsorption performance of the solid adsorbent generally increases with the initial concentration of the adsorbate. This is due to the increase in driving force for transporting the adsorbate molecules from aqueous phase to the adsorbent surface (Ahmad et al., 2016; Kallel et al., 2016). The number of collisions between the adsorbate molecules and the adsorbent functional groups also rises as the initial concentration increases, which resulted in the escalation of the adsorption capacity (Hadi et al., 2015).

Maneerung et al. (Maneerung et al., 2016) observed that the amount of RhB adsorbed on activated-GC derived from woody biomass increased with the initial concentration. At 25 °C, the equilibrium adsorption capacity of activated-GC significantly increased from 132 to 232 mg/g when the initial RhB concentration was increased from 13 to 28 mg/L. The increase in adsorption capacity was due to a higher concentration gradient or stronger driving force between the liquid and GC solid phases at a higher initial RhB concentration. This in turn led to an increase in adsorption capacity. In general, the initial concentration plays a crucial role in overcoming mass transfer resistance of adsorbate molecules between liquid and solid phases during adsorption (Ab Aziz et al., 2023; Kwon et al., 2011).

In the studies of ATN adsorption by GGSWAC, Ahmad et al. (Ahmad et al., 2020) observed a similar trend where the adsorption uptake of ATN molecules on the adsorbent increased from 25.65 to 120.94 mg/g as the initial concentration of ATN increased from 50 to 300 mg/L. This was due to the greater mass transfer driving force at higher initial concentrations which helped to overcome the mass transfer resis-

tance of ATN between the liquid and solid phases. The higher initial concentrations resulted in more ions competing for available sites on the surface of the adsorbent, as reported by Azari et al. (Azari et al., 2021), thus leading to a higher ATN adsorption capacity. These findings were consistent with the adsorption studies conducted by To et al. (To et al., 2017) and Fu et al. (Fu et al., 2020). Additionally, in the study on iron, copper, and nickel removal, Runtti et al. (Runtti et al., 2014) observed that the adsorbent reached its saturation point at higher initial metal concentrations and could no longer accommodate further sorption due to the absence of available sites.

Meanwhile, contact time can be defined as the agitation time needed for the adsorbent–adsorbate system to achieve steady state. The adsorption process can be described by few steps; (1) film diffusion (mass transfer from the liquid phase to the adsorbent surface across the liquid film), (2) intraparticle diffusion (diffusion within the pores of adsorbent) and (3) surface reaction (adsorption on the surface of adsorbent) (Tan and Hameed, 2017; Choudhary et al., 2020). The equilibrium time commonly varies according to adsorbent pore structure and particle size, type of the adsorbate, adsorbate concentration, solution temperature and pH. Hadi et al. (Hadi et al., 2015) reported that the equilibrium time for the mesoporous adsorbent is much lesser than the microporous adsorbent. Additionally, the tinier particle size of adsorbent requires shorter equilibrium time compared to adsorbent with larger particle size (Bohli et al., 2013).

The adsorption experiment to determine the adequate adsorption time of RhB by activated GC was conducted by Maneerung et al. (Maneerung et al., 2016) at room temperature using 5 mg of activated GC and 100 mL of 20 mg/L RhB solution (pH 7). The amount of adsorbed RhB (Q_t) increased rapidly with the contact time up to 180 min, after

Table 7 Adsorption mechanisms of various pollutants onto GC.

Category	Feedstock	Pollutant	Mechanism	Reference
Ions	Pine and spruce woodchip	SO ₄ ²⁻	physical pore filling, electrostatic interactions	(Runtti et al., 2016)
	Pine and spruce woodchip	NO ₃ ³⁻	physical pore filling, electrostatic interactions	(Kilpimaa et al., 2015)
	Pine and spruce woodchip	Fe ²⁺ , Cu ²⁺ and Ni ²⁺	electrostatic attraction, ion-exchange, adsorption–precipitation, hydrogen bonding, and chemical interaction	(Runtti et al., 2014)
	Gasified rice waste	Cr ³⁺	ion exchange, physical pore filling, precipitation, electrostatic interactions	(Godinho et al., 2017; Dias, 2018)
Dyes	<i>Glyricidia sepium</i>	MG	H-bond, π-π interaction, electrostatic interaction	(Ahmad et al., 2020)
	<i>Woodchip</i>	MG	H-bond, π-π interaction, electrostatic interaction	(Ahmad et al., 2020)
	Mesquite wood chips	RhB	H-bond, electrostatic interaction	(Maneerung et al., 2016)
	Municipal solid waste	CR & CV	H-bond, π-π interaction, hydrophobic interactions, electrostatic interaction	(Jung et al., 2019)
Emerging contaminant	<i>Hevea brasiliensis</i> root	MG	H-bond, π-π interaction, electrostatic interaction	(Ahmad et al., 2021)
	<i>Glyricidia sepium</i>	ATN	H-bond, π-π interaction, electrostatic interaction, London dispersion force	(Ahmad et al., 2020)
	Spruce woodchip	DCF	hydrophobic and π-electron-donor–acceptor & π-cation interactions, pore-size effects, electrostatic interaction & H-bond	(Back et al., 2020)

which it slowly increased until it reached equilibrium at maximum adsorption capability at ~ 240 min of contact time. This is because the initial adsorption rate was rapid due to the high number of vacant sites of the activated GC for adsorption, and then it slowly increased due to the saturation of active sites for adsorption. The maximum adsorption capacity at equilibrium of the activated GC prepared was approximately 215.7 mg/g as shown in Fig. 2.

Similarly, Runtti et al. (Runtti et al., 2016) reported that the initial stage of the sorption experiment had a higher rate of sulphate ion removal due to the greater number of available adsorption sites. The optimal sulphate removal efficiency (97.6%) and sorption capacity (10.3 mg/g) were achieved in approximately one minute, after which there was a slight decrease in the removal efficiency.

8.2. Effect of temperature

Temperature is another important parameter that may affect adsorption by affecting solubility and molecular interactions with solid particles. The solution temperature can either improve or reduce the adsorption performance depending on the nature of the adsorbate-adsorbent interaction, whether exothermic or endothermic process (Chen, 2022). In ACE adsorption using GC from pine wood, the increase in adsorption capacity due to temperature was observed by Galhetas et al. (Galhetas et al., 2014), which is consistent with previously reported data (Ahmad et al., 2020; Ahmad et al., 2021; Ahmad et al., 2020; Ahmad et al., 2020), demonstrating a temperature dependence that is a characteristic of an endothermic process. The authors also explained that the relationship between the dimension of ACE species present in solution and the micropore size network of the GC samples can account for this phenomenon. At lower temperatures, the critical dimension of ACE monomers is close to the opening of the pores corresponding to the maximum of the micropore size distribution of the lab-made sample. However, with an increase in temperature from 20 to 40 °C, the vibration energy of the molecules increases, leading to an activation of adsorption. This favours the accessibility of the species to the microporosity with widths near to the critical dimensions of the molecule, resulting in an increase in monolayer adsorption capacity.

On the contrary, Maneerung et al. (Maneerung et al., 2016) found that the adsorption capacity of RhB slightly decreased

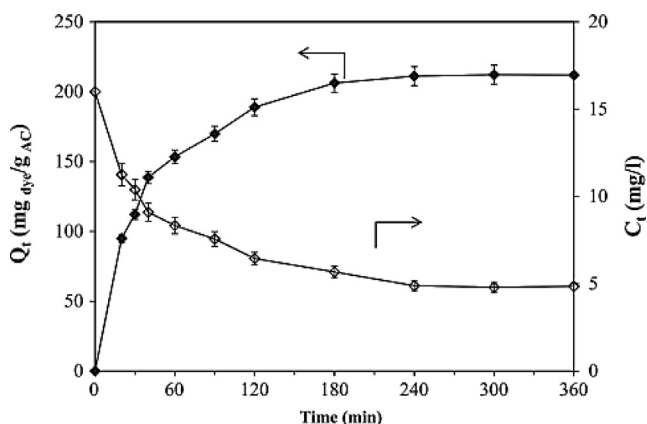


Fig. 2 Effect of contact time (Maneerung et al., 2016).

as the temperature increased. For example, when the initial concentration was kept constant at 22 mg/L, the amount of RhB adsorbed on the GC decreased from 210.2 to 196.4 mg/g as the temperature increased from 25 to 60 °C. This observation indicates that the adsorption of RhB onto the GC is an exothermic process.

The study of temperature is vital in evaluating the thermodynamic parameters such as the change of Gibbs free energy (ΔG°), enthalpy (ΔH°) and entropy (ΔS°), which can provide the information related to the adsorption nature (Moralh et al., 2018). An accurate estimation of these parameters relies on the appropriate determination of the equilibrium constant, K_C . The thermodynamic parameters can be estimated using K_C values obtained from adsorption-isotherm constants or the partition coefficient (Ribas, 2014; Rodrigues et al., 2011). However, several factors need to be considered thoroughly to obtain a reliable value of these thermodynamic parameters; (1) The K_C value must be unitless. (2) The van't Hoff linear regression coefficient (R^2) must be high. (3) The adsorbate concentration used in the adsorption equilibrium study are low or high (Nguyen et al., 2017). Since the K_C values can be estimated from several methods, significant variation in the thermodynamic parameters can be found. Hence, the most reliable approach should be studied so that the determined thermodynamics parameters are relevant.

Rangabhashiyam et al. (Rangabhashiyam et al., 2018) used the distribution constant, K_d to estimate the thermodynamic properties of MG adsorption onto Carica papaya wood (CPW). The authors estimated K_d value from the intersection of $\ln(q_e/C_e)$ versus C_e plot. The results showed a declining trend in the value of Gibbs free energy with increasing temperature, suggesting that adsorption of MG was preferred at higher temperature. The results of the enthalpy change revealed that the MG adsorption process was endothermic, and the positive values of the entropy change indicated the increase randomness in the system.

The estimation of K_C values from Langmuir isotherm, K_L for MG, MB, and RhB adsorption were employed by Geçgel et al. (Geçgel et al., 2016), who used AC obtained from waste *Elaeagnus* stone. They reported the negative values of Gibbs free energy, which revealed the spontaneity of the process; the positive values of entropy change indicating the increase in the randomness in the system; and the positive values of enthalpy which reconfirm that the adsorption of MG was endothermic. Similar approach has been performed by Qu et al. (Qu et al., 2019), who evaluated the MG adsorption using apricot-AC, coconut-AC, peach-AC and coal-AC. The thermodynamic results obtained by Qu et al. (Qu et al., 2019) were in good agreement with Geçgel et al. (Geçgel et al., 2016). In contrast, Saygılı & Güzel (Saygılı and Güzel, 2015) calculated the thermodynamic properties of CR and MG adsorption using distribution coefficient with $K_d = Q_m K_L$ with unit of L/g, which was different from those of K_L (L/mg). The results for thermodynamic properties were in good agreement with other researchers with high value of R^2 .

8.3. Effect of pH

A pH of the solution is another important factor that affect the adsorption capacity. The pH value can influence the ionization degree of the adsorbate and metal ion speciation in a solution.

A solution's pH affects the degree of the adsorption. H^+ and OH^- ions are commonly adsorbed, thus affecting the adsorption process by dissociating the functional groups on the active sites of the adsorbent surface, resulting in a shift in the kinetics of reaction and in the properties of equilibrium (Rathi and Kumar, 2021).

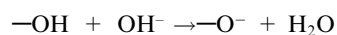
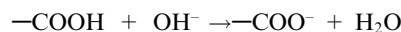
The influence of pH can also be clarified in terms of point of zero charge (pH_{PZC}) value. At $pH < pH_{PZC}$, the adsorbent surface becomes mainly positively charged which tends to attract the anionic adsorbate owing to the increase in the number of the positively charged groups at the surface of the adsorbent, leading to the increase in adsorption of the adsorbate molecules to the surface of the adsorbent. In contrast, the adsorbent surface becomes deprotonated at $pH > pH_{PZC}$ due to the availability of large number of negatively charged ions on the surface of adsorbent, resulting in the electrostatic repulsion between the negatively charged adsorbent surface and the anionic adsorbate. For instance, Ahmad et al. (Ahmad et al., 2020) reported that, at pH value lower than pH_{PZC} ($pH < 4.8$), the GC surface were positively charged while at pH value greater than pH_{PZC} ($pH > 4.8$), the surfaces became negatively charged. Therefore, when the pH is above pH_{PZC} ($pH > 4.8$), the GC surface possessed the net negative charge and promoted the electrostatic attraction with positively charged ATN solution. Hence the adsorption uptake increased from 67.65 to 74.71 mg/g at pH 4 and pH 8 as depicted in Fig. 3. However, at pH above the pK_a value, ATN molecules were deprotonated and became neutral, thus causing a declining trend in ATN uptake at pH 10 to 12. Similar trend was reported by Haro et al. (Haro et al., 2017), To et al. (To et al., 2017), Fu et al. (Fu et al., 2020) and Chang (Chang et al., 2019).

Sharma et al. (Sharma, 2019) found that the maximum MG adsorption by AC derived from *Pinus roxburghii* cone occurred at pH 6 with pH_{PZC} value of 8.4. At pH 6 (below the pH_{PZC}), the surface of AC was positively charged, while the MG molecules was either neutral or slightly negatively charged, thus demonstrating the greatest interactions between AC and MG molecules, leading to high adsorption performance.

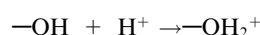
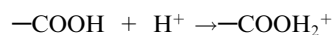
Meanwhile, the effect of pH was described using chemical equation by Maneerung et al. (Maneerung et al., 2016), who studied the RhB removal using activated GC. Under the basic condition, the hydroxyl ($-OH$) groups and carboxylic ($-COOH$) groups on the surface of GC were deprotonated and became more negatively charged, which led to the increase in the electrostatic interaction between the negatively charged

GC and the positively charged RhB molecule. In contrast, under the acidic condition, the hydroxyl groups and carboxyl functional groups of the GC as well as the carboxyl functional groups of RhB molecules were protonated and became more positively charged. Hence the adsorption capability declined owing to the strong electrostatic repulsion between the positively charged RhB molecules and the positively charged GC.

Under basic condition:



Under acidic condition:



Under neutral condition, Maneerung et al. (Maneerung et al., 2016) added that RhB molecules were mostly adsorbed on the surface of GC via hydrogen bonding between carboxylic ($-COOH$) groups of RhB molecules and both hydroxyl ($-OH$) groups and carboxylic ($-COOH$) groups present on the surface of GC. They finally concluded that the basic condition was more favorable for the adsorption of cationic dye-RhB by the prepared GC.

According to Ravenni et al. (Ravenni et al., 2020), the adsorption of cations or anions, influenced by solution pH, is related to the zeta potential of the GC surface, which measures the electric potential at the interface between the adsorbent and the surrounding solution. When the GC surface has a positive or negative zeta potential, there is an electrostatic attraction or repulsion between the ionic dyes and the surface. For instance, if the solution pH is higher than the pH_{PZC} , the GC surface becomes negatively charged, facilitating the adsorption of positively charged ions of cationic dyes. This is why cationic-MB is adsorbed more efficiently and with faster kinetics compared to anionic-AM on the adsorbents tested.

Meanwhile, Jung et al. (Jung et al., 2019) observed that the equilibrium adsorption capacity, q_e , for anionic dye-CR adsorption decreased with an increase in pH, indicating the potential presence of negatively charged species in the GC. On the other hand, the adsorption of cationic dye-CV showed an increasing trend in q_e as the initial solution pH increased because of the higher concentration of positively charged (H^+) ions in solution at low pH, leading to increased competition for available adsorption sites.

9. Adsorption isotherm & kinetic

The adsorption isotherm models provide essential data on the adsorbent surface characteristic, adsorbent affinities towards adsorbate, adsorbent uptake capacity and adsorption mechanisms. Most of the researchers employed two and three parameter isotherm models for monolayer adsorption system, including Langmuir, Freundlich, Sips, Dubinin-Radushkevich (D-R), Redlich Peterson (R-P) and Temkin. Other monolayer models such as Hills, Koble-Corrigan (K-C), Radke-Prausnitz Radke, Toth, Fritz-Schlunder (F-S), Khan, Jossens, Flory-Huggins, Baudu and multilayer models including Aranovich, Brunauer-Emmett-Teller (BET), n-BET, Anderson, Dubinin-Serpinsky, Frenkel-Halsey-Hill and

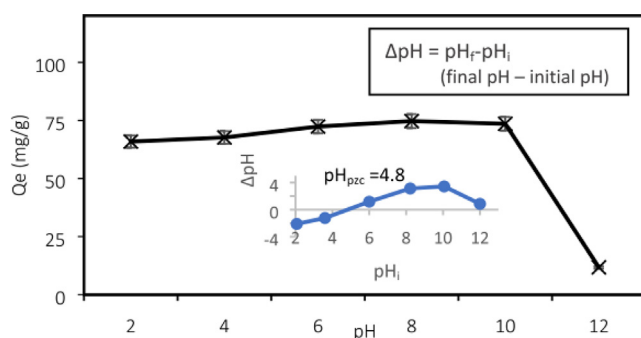


Fig. 3 Effect of pH (Ahmad et al., 2020).

Guggenheim Anderson de-Boer (GAB) (Saadi et al., 2015) were rarely reported or almost absence in the literature for adsorption isotherm study. This could be due to more complex equation consisting of more than three parameters which requires the optimization of non-linear equations. Limited number of studies has been found applying multilayer isotherm such as BET model equation for phenol (Horváth et al., 2017), dye (Scheufele, 2016) and emerging contaminant (Sotelo et al., 2012) adsorption. The correct form of BET isotherm for modeling liquid phase adsorption was discussed by Ebadi et al (Ebadi et al., 2009). According to BET model, the second, third, and subsequent layers have similar amount of adsorption energy and are unaffected by adsorbent-adsorbate interactions. In contrast, the first layer energy differs from other layers. The adsorption layers tend to become infinity at saturation concentration. Scheufele et al. (Scheufele, 2016) for instance, employed the multilayer BET equation for the reactive blue 5G dye removal from aqueous solution with high R^2 value of 0.9568–0.9967 and concluded that the adsorption of RB5G showed a multilayer adsorption behavior. Another study using BET isotherm model was reported by Sotelo et al. (Sotelo et al., 2012), who investigated the adsorption of isoproturon and ATN in batch and continuous mode of operation. The equilibrium state of batch adsorption was found after 25 h and the isotherm data ideally fitted to BET model ($R^2 = 0.9962$) with monolayer adsorption capacity, $q_{m,BET}$ of 80.4 mg/g.

The adsorption kinetic models provide insights over the dynamics of adsorption of adsorbate onto the adsorbent and gave the information on the ruling adsorption mechanism. Pseudo-first order (PFO), Pseudo-second order PSO and Elovich model equations were mostly reported for various pollutants adsorption due to the simplicity of the equations. In short, the appropriate models must be carefully applied for better insight on the thermodynamic properties as well as the adsorption mechanism that ruled the process. Table 8 and Table 9 show several isotherm and kinetic model equations that had been widely used in liquid adsorption.

Table 10 indicates the fitted isotherm and kinetic models for liquid adsorption by GC. In the studies of MG and ATN adsorption by various GCs conducted by Ahmad et al. (Ahmad et al., 2020; Ahmad et al., 2021; Ahmad et al., 2020; Ahmad et al., 2020), Langmuir, Freundlich, D-R, Temkin, R-P, K-C, F-S, n-BET and Toth isotherm models were employed. They found that n-BET model fitted all the experimental data very well. This model assumes there are a maximum number of layers, n that can be adsorbed onto the internal surface (Saadi et al., 2015). Number of layers ($n = 1, 2, 3, \dots, nth$) can be defined as follows: (See Fig 4)

The n value of less than 2 for MG removal (Ahmad et al., 2020; Ahmad et al., 2020), which was attributed to monolayer adsorption, showed a good agreement with the monolayer adsorption isotherm models, such as F-S ($R^2 = 0.99$), R-K ($R^2 = 0.97$), Toth ($R^2 = 0.97$), Sips ($R^2 = 0.97$), Langmuir ($R^2 = 0.97$), K-C ($R^2 = 0.97$), D-R ($R^2 = 0.94$), and Temkin ($R^2 = 0.93$) with reasonable values of R^2 . In addition, Ahmad et al. (Ahmad et al., 2020) also reported that the MG adsorption occurred at the specific homogeneous sites of the GGSWAC as supported by the values of α_{RP} ; n_s , n_{Toth} and k_{KC} in R-P, Sips, Toth and K-C isotherm models respectively, which were close to unity. The system is heterogenous when

these values deviate from 1, while the values close to 1 describe a homogeneous system. Meanwhile, the D-R model was also employed by Ahmad et al. (Ahmad et al., 2020; Ahmad et al., 2020) to evaluate the energy of adsorption. The energy of adsorption, E , was applied to judge the adsorption type; when $1 < E < 8$ kJ/mol, the adsorption is categorized as physical process, when $8 < E < 16$ kJ/mol, the adsorbate is absorbed by ion exchange, and when $E > 16$ kJ/mol, the chemical adsorption involved. The low sorption energy, E (< 8 kJ/mol), provided from D-R indicated physisorption.

The heterogeneity of the system can also be described by Bi-Langmuir isotherm equation as employed by Runtti et al. (Runtti et al., 2016). The model assumes that there are two favoured adsorption sites on the surface and was first suggested by Graham (Graham, 1953). Runtti et al. (Runtti et al., 2016) who studied sulphate removal using $FeCl_3$ -activated GC from 150 kW downdraft gasifier operating at 1000 °C, reported Bi-Langmuir model ideally fitted the experimental data ($R^2 = 0.98$), followed by Sips ($R^2 = 0.96$), Freundlich ($R^2 = 0.96$) and Langmuir ($R^2 = 0.75$), suggesting heterogeneous adsorption of SO_4^{2-} anions onto the surface of GC with two different types of adsorption sites. This result showed a good agreement with the heterogeneity factors in Sips ($n_s = 0.2$), and Freundlich ($1/n = 0.11$) as their values deviate from unity, indicating a heterogenous adsorption site. In kinetic study, Runtti et al. (Runtti et al., 2016) employed both PFO and PSO models and reported that the R^2 value of the PFO kinetic model was lower than that of the PSO model. In addition, experimental uptake values ($q_{e,exp}$) were not reasonable in regard to the calculated values ($q_{e,calc}$). Therefore, the PSO kinetic model was selected as the best-fit model ($R^2 = 0.99$).

Pessôa et al. (Pessôa, 2019) and Godinho et al. (Godinho et al., 2017) reported that Sips model greatly described the adsorption of MB and Cr^{3+} ions onto GC derived from açai berry seeds and rice husk, respectively. Based on kinetic data, the adsorption of Cr^{3+} ions fitted well to the PSO model with R^2 of 0.96, indicating that ion exchange might have occurred during the adsorption process (Godinho et al., 2017). Meanwhile, Pessôa et al. (Pessôa, 2019) employed pseudo-n-order (PNO) model together with PFO and PSO. They reported that all models accurately predicted the MB adsorption with R^2 of 0.996, 0.996 and 0.994 for PNO, PSO and PFO, respectively. The order factor (n) value in PNO were 2.26, indicating that the adsorption was equivalent to the second-order model, which was supported by the high value of R^2 for PSO. However, Pessôa et al. (Pessôa, 2019) did not further elaborated on the adsorption mechanism based on the findings in isotherm and kinetic studies.

Other researchers revealed that the adsorption of RhB (Maneerung et al., 2016), phosphate & nitrate (Kilpimaa et al., 2015; Kilpimaa et al., 2014), nickel, iron & copper (Runtti et al., 2014), ACE & caffeine (Galhetas et al., 2014; Galhetas et al., 2014) and chromium (III) (Dias, 2018) followed Langmuir adsorption isotherm and PSO kinetic models, manifesting that the adsorbate molecules formed monolayer coverage on the prepared GC, which is homogenous in nature. It can be concluded that every adsorption sites of the GC have the same adsorption energy. In addition, Dias et al. (Dias, 2018) emphasized that the adsorption of chromium (III) was mostly driven by ion exchange rather than by physical adsorption.

Table 8 Isotherm model equations (Ahmad et al., 2020).

Isotherm model	Equation	Parameter	Model Description	Ref
Freundlich	$q_e = K_F C_e^{1/n}$	$K_F, 1/n$	An empirical model assuming that the distribution of the heat on the adsorbent surface is non-uniform.	(Freundlich, 1906)
Langmuir	$q_e = \frac{q_{max} K_L C_e}{1 + K_L C_e}$	q_{max}, K_L	Assuming monolayer adsorption occurs on the solid surface with identical homogeneous sites.	(Langmuir, 1918)
Dubinin-Radushkevich (D-R)	$q_e = q_{DR} \exp\left[\frac{(RT \ln(1+1/C_e))^2}{-2E^2}\right]$	q_{DR}, E	Often used to estimate the characteristic porosity in addition to the apparent free energy of adsorption.	(Kutluay et al., 2019)
Temkin	$q_e = \frac{RT}{b_T} \ln(K_T C_e)$	b_T, K_T	Heat of adsorption decrease linearly rather than logarithmically due to adsorbate-adsorbent interactions.	(Ayawei et al., 2017)
Redlich-Peterson (R-P)	$q_e = \frac{K_R C_e}{1 + A_R C_e^{\alpha_{RP}}}$	K_R, A_R, α_{RP}	Valid when the mechanism of adsorption is a hybrid and does not follow ideal monolayer adsorption.	(Saravanan et al., 2018)
Sips	$q_e = \frac{q_S K_S C_e^{n_S}}{1 + K_S C_e^{n_S}}$	q_S, K_S, n_S	Valid for predicting the heterogeneous adsorption systems and localized adsorption without adsorbate-adsorbate interactions.	(Popoola et al., 2019)
Koble-Corrigan (K-C)	$q_e = \frac{A_{KC} C_e^{k_{KC}}}{1 + B_{KC} C_e^{k_{KC}}}$	A_{KC}, B_{KC}, k_{KC}	Incorporates both Langmuir and Freundlich isotherms. Mostly applied for heterogeneous adsorbent surface.	(Wakkel et al., 2019)
Fritz-Schlünder (F-S)	$q_e = \frac{A C_e^\alpha}{1 + B C_e^\beta}$	A, B, α, β	An empirical equation which can fit a wide range of experimental data.	(Fritz and Schlünder, 1974)
n-layer BET	$q_e = q_m \frac{K_S C_e [1 - (n_{BET} + 1)(K_{L,BET} C_e)^{n_{BET}} + n_{BET} (K_{L,BET} C_e)^{n_{BET} + 1}]}{(1 - K_{L,BET} C_e) \left[1 + \left(\frac{K_S}{K_{L,BET}} - 1 \right) K_L C_e - \left(\frac{K_S}{K_{L,BET}} \right) (K_{L,BET} C_e)^{n_{BET} + 1} \right]}$	$q_m, K_S, K_{L,BET}, n_{BET}$	Assuming that there are a maximum n layers that can be adsorbed onto the internal surface of adsorbent.	(Scheufele, 2016)
Toth	$q_e = \frac{q_{mToth} k_{Toth} C_e}{[1 + (k_{Toth} C_e)^{n_{Toth}}]^{1/n_{Toth}}}$	$q_{mToth}, k_{Toth}, n_{Toth}$	Useful in describing heterogeneous adsorption systems.	(Toth, 1971)

The multilayer adsorption (with limited number of layers, n) was reported by Ahmad et al (Ahmad et al., 2021; Ahmad et al., 2020) for the removal of MG and ATN based on the excellent fitting ($R^2 = 0.98-0.99$) in the n-BET isotherm equation as well as the number of layer predicted by this model ($n \geq 2$). The maximum number of layers, n equal to 3, 6, 5 and 2.5, 2.1, 2.7 at 30, 45 and 60 °C for MG and ATN adsorption respectively. The finding was further proven with the heterogeneity value of n_S predicted by Sips which were far from unity ($n_S = 2.19$), suggesting heterogenous distribution of the adsorption sites. In the kinetic study, Ahmad et al. (Ahmad et al., 2020; Ahmad et al., 2021; Ahmad et al., 2020;

Ahmad et al., 2020) applied PFO, PSO, Elovich and Avrami models and all the data fitted to Avrami model very well ($R^2 = 0.98-0.99$). Avrami model is generally used for unusual adsorption kinetic quantities when the adsorption rate is very slow and/or presents more than one adsorption mechanism. The Elovich model showed poor fitting with R^2 values of 0.17–0.65 (Ahmad et al., 2021; Ahmad et al., 2020; Ahmad et al., 2020), confirming that this model was not appropriate to describe the rate of MG adsorption, and the MG removal was not governed by chemisorption. In contrast, some of the kinetic data for ATN adsorption (Ahmad et al., 2020) correlated well with Elovich model, suggesting the possibility of

Table 9 Non-linear kinetic model equations (Ahmad et al., 2020).

Kinetic model	Equation	Parameter	Description	Ref
Pseudo-first order (PFO)	$q_t = q_e [1 - \exp(-k_1 t)]$	q_e, k_1	The change in rate of the solute uptake with time is directly proportional to the difference in saturation concentration and the solute uptake with time.	[191]
Pseudo-second order (PSO)	$q_t = \frac{k_2 q_e^2 t}{1 + k_2 q_e t}$	q_e, k_2	The rate limiting step are chemisorption involves forces by sharing or exchanging electrons between the adsorbent and the adsorbate.	(Ho and Mckay, 1999)
Elovich	$q_t = \frac{1}{\beta} \ln(1 + \alpha_E \beta t)$	α_E, β	Commonly used in chemisorption processes.	(Low, Jun, 1960; Agbor Tabi, 2022)
Avrami	$q_t = q_e \{1 - \exp[-(k_{AV} t)^{n_{AV}}]\}$	q_e, k_{AV}, n_{AV}	Used to verify specific changes of kinetic parameters as functions of temperature and reaction time. For unusual adsorption kinetic quantities when the adsorption rate is very slow and presents more than one adsorption mechanism.	(Avrami, 1939)

Table 10 Isotherm & Kinetic Models for GC.

Feedstock	Application	Adsorption capacity (mg/g)	Kinetic		Isotherm		Reference
			Model	R ²	Model	R ²	
<i>Hevea brasiliensis</i> root	MG	259.49	Avrami	0.999	n-BET	0.988	(Ahmad et al., 2021)
	<i>Glyricidia sepium</i>	230.47	Avrami	0.999	Fritz-Schlünder	0.992	(Ahmad et al., 2020)
Woodchip	ATN	163.0	Avrami	0.998	n-BET	0.998	(Ahmad et al., 2020)
	MG	226.06	Avrami/PFO	0.987	Fritz-Schlünder	0.992	(Ahmad et al., 2020)
Mesquite wood	RhB	189.83	PSO	0.995	Langmuir	0.991	(Maneering et al., 2016)
Açai berry seeds	MB	93.23	PNO	N/A	Sips	0.998	(Pessôa, 2019)
Woodchip	MB	25.1	PFO	0.998	N/A	N/A	(Ravenni et al., 2020)
	AM	25.3	PSO	0.992			
Municipal Solid waste	CR	49.7	PSO	0.932	Redlich-Peterson	0.952	(Jung et al., 2019)
	CV	356	PSO	0.962		0.979	
Pine and spruce	SO ₄ ²⁻	19.55	PSO	0.999	Bi-Langmuir	0.980	(Runtti et al., 2016)
Pine and spruce	PO ₄ ³⁻	20.5	PSO	0.997	Langmuir	0.998	(Kilpimaa et al., 2015; Kilpimaa et al., 2014)
	NO ₃ ⁻	80		0.999		0.992	
	Ni ²⁺ , Fe ²⁺ , Cu ²⁺	18.2, 20.5, 23.1	PSO	0.999	Langmuir	0.979	(Runtti et al., 2014)
Pine	ACE	434.8	PSO	0.999	Langmuir	0.990	(Galhetas et al., 2014; Galhetas et al., 2014)
	Caffeine	476.2		0.999		0.999	
Spruce woodchip	DCF	35.09	PSO	0.890	Freundlich	0.980	(Back et al., 2020)
Rice Husk	Cr ³⁺	21.1	PSO	0.966	Sips	0.956	(Godinho et al., 2017)
50% w/w RH + 50% w/w RS	Cr ³⁺	8.51	N/A	N/A	N/A	N/A	(Dias, 2018)
	Cr ³⁺	6.2	PSO	N/A	Langmuir	0.999	

RH = rice husk, RS = rice straw, PE = polyethylene, RhB = rhodamine B, AM = amanth dye, CR = congo red dye, CV = crystal violet dye, ATN = atenolol, ACE = acetaminophen, DCF = diclofenac, MB = methylene blue dye, MG = malachite green dye, PFO = Pseudo-first order, PSO = Pseudo-second order, PNO = Pseudo-n-order.

chemisorption involved. Ahmad et al. (Ahmad et al., 2020) further concluded that the overall mechanism of ATN adsorption was ruled by both film diffusion and chemisorption based on the results from Weber & Moris IPD, Boyd and diffusion-chemisorption models.

The adsorption of CR and CV (Jung et al., 2019) were ideally described by R-P model with R² of 0.95 and 0.98, respectively. The values of α_{RP} in the Redlich-Peterson models were close to 1, which can be reduced to the Langmuir isotherm model, manifesting a monolayer adsorption, which indicated

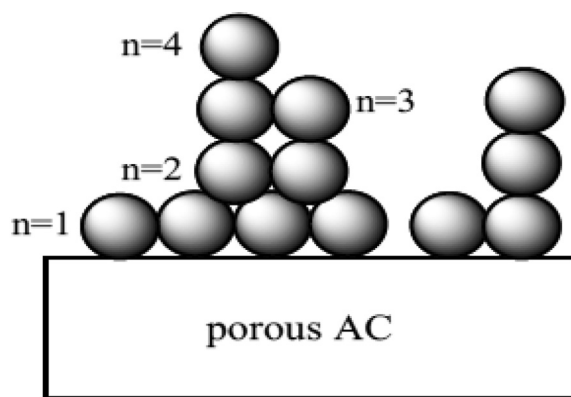


Fig. 4 Number of layers, n .

the adsorbent-adsorbate interaction. In addition, some pore filling phenomena were depicted by D-R model ($R^2 = 0.91$) for CV removal with adsorption energy ascribed to physisorption ($E < 8$ kJ/mol). The kinetic data for both CR and CV adsorption fitted well to PSO, suggesting chemisorption. Thus, it can be concluded that CR and CV adsorption had both physisorption and chemisorption contributions.

10. Rate controlling steps of adsorption

It is well known that during the adsorption of adsorbate over a porous adsorbent, the following three consecutive steps were taken place: (1) transport of the ingoing adsorbate ions to external surface of the adsorbent, (2) transport of the adsorbate ions within the pores of the adsorbent and (3) adsorption of the ingoing adsorbate ions on the internal surface of the adsorbent. Out of these three processes, the third process is considered to be very quick and is not the rate-limiting step in the adsorption of organic compounds (Karthikeyan et al., 2010). Hence, the adsorption process is governed either by external diffusion, internal diffusion or by both types of diffusions. Most of the researchers only considered these two processes to determine the slowest steps in adsorption process (Wakkal et al., 2019; Bhattacharyya and Ray, 2015; Maia et al., 2019; Oyelude et al., 2018; Sewu et al., 2017; Sy et al., 2017). The Weber and Morris IPD model, the Boyd kinetic model are the two models that were commonly applied to evaluate whether intraparticle or film diffusion is the rate controlling step. However, for complex processes that involve chemical reaction, diffusion-chemisorption model was also applied. For example, To et al. (To et al., 2017) used the Weber and Morris IPD, Boyd kinetic and the diffusion-chemisorption model equations to investigate the adsorption mechanism of ATN adsorption onto activated PKS. The ATN adsorption ideally fitted to the diffusion-chemisorption model ($R^2 \geq 0.998$) suggesting that the ATN adsorption was governed by diffusion and chemisorption. To et al. concluded that the binding mechanism of ATN adsorption onto the adsorbent was related to hydrogen bonding.

Similar models was employed by Choudhary et al. (Choudhary et al., 2020), whom investigated the removal of MG using *Opuntia ficus-indica*-derived AC. They computed the diffusion-chemisorption model, together with Weber and Morris IPD and Boyd kinetic models and found that the kinetic data fitted well to diffusion-chemisorption model

($R^2 \geq 0.99$) indicating that both diffusion and chemisorption ruled the adsorption process. This is in agreement with the results reported by Ahmad et al. for ATN adsorption by gasified *Glyricidia sepium* (Ahmad et al., 2020). The data revealed that the overall mechanism of ATN adsorption was ruled by both film diffusion and chemisorption based on high correlation coefficient R^2 ranging from 0.9984 to 1.000.

11. Conclusion and future prospects

Previously published papers concluded that both the physical and chemical properties of sorbents play important roles in the adsorption process. Physical properties such as S_{BET} and TPV are critical factors that influence adsorption efficiency. Chemical properties such as the presence of oxygen-rich functional groups and aromatic groups on the surface of char are responsible for providing strong active sites for adsorption.

While many scholars have studied the adsorption process using other materials as adsorbents, gasification residues have been rarely researched. Owing to its good physicochemical properties, high adsorption capability, and new added-value offered, GC residue presents good application prospects as alternative feedstock for AC.

Owing to the good physicochemical properties of GC residues, their application for adsorption should be further investigated. The literature on the applications of GC residues for adsorption is somewhat limited to the adsorption of dyes and heavy metals. Furthermore, studies on the removal of pharmaceutical compound have been extremely rare. Additionally, studies on the activation parameters (i.e: temperature, impregnation ratio of activation agent, activation duration), adsorption conditions (i.e: pH, initial sorbate concentration, temperature, sorbent dosage), kinetics (i.e: pseudo first order, pseudo second order), thermodynamics (ΔH , ΔG , ΔS), and regeneration should be conducted to analyse the adsorption mechanism involved. The effects of these parameters on the adsorption performance of GC should be examined by analysing the optimal experimental conditions. In addition, an economic analysis of the production of AC from GC should be conducted. The findings of the studies cited in this paper are crucial for designing pilot-plant scale adsorption columns to assess the feasibility of GC at industrial level.

Declaration of Competing Interest

The authors declare that they have no known competing financial interests or personal relationships that could have appeared to influence the work reported in this paper.

Acknowledgments

The authors thankfully acknowledge the support obtained from Ministry of Higher Education (MOHE), Universiti Malaysia Perlis (UniMAP), Universiti Sains Malaysia (USM) and Intel Microelectronics (M) Sdn Bhd in form of scholarship and facilities given to the corresponding author.

References

- Ab Aziz, N.A.H., Md Ali, U.F., Ahmad, A.A., Mohamed Dzahir, M. I.H., Khamidun, M.H., Abdullah, M.F., 2023. Non-functionalized

- oil palm waste-derived reduced graphene oxide for methylene blue removal: Isotherm, kinetics, thermodynamics, and mass transfer mechanism. *Arab. J. Chem.* 16 (1), 104387. <https://doi.org/10.1016/j.arabjc.2022.104387>.
- Abbas, M., Trari, M., 2015. Kinetic, equilibrium and thermodynamic study on the removal of Congo Red from aqueous solutions by adsorption onto apricot stone. *Process Saf. Environ. Prot.* 98, 424–436. <https://doi.org/10.1016/j.psep.2015.09.015>.
- Abdelhadi, S.O., Dosoretz, C.G., Rytwo, G., Gerchman, Y., Azaizeh, H., 2017. Production of biochar from olive mill solid waste for heavy metal removal. *Bioresour. Technol.* 244 (June), 759–767. <https://doi.org/10.1016/j.biortech.2017.08.013>.
- Abdulrazzaq, H., Jol, H., Husni, A., Abu-Bakr, R., 2014. Characterization and stabilisation of biochars obtained from empty fruit bunch, wood, and rice husk. *BioResources* 9 (2), 2888–2898. <https://doi.org/10.15376/biores.9.2.2888-2898>.
- Agbor Tabi, G. et al., 2022. Non-linear modelling of the adsorption of Indigo Carmine dye from wastewater onto characterized activated carbon/volcanic ash composite. *Arab. J. Chem.* 15, (1). <https://doi.org/10.1016/j.arabjc.2021.103515> 103515.
- Ahmad, M. et al., 2014. Speciation and phytoavailability of lead and antimony in a small arms range soil amended with mussel shell, cow bone and biochar: EXAFS spectroscopy and chemical extractions. *Chemosphere* 95, 433–441. <https://doi.org/10.1016/j.chemosphere.2013.09.077>.
- Ahmad, M.A., Afandi, N.S., Adegoke, K.A., Bello, O.S., 2016. Optimization and batch studies on adsorption of malachite green dye using rambutan seed activated carbon. *Desalin. Water Treat.* 57 (45), 21487–21511. <https://doi.org/10.1080/19443994.2015.1119744>.
- Ahmad, A.A., Zawawi, N.A., Kasim, F.H., Inayat, A., Khasri, A., 2016. Assessing the gasification performance of biomass: A review on biomass gasification process conditions, optimization and economic evaluation. *Renew. Sustain. Energy Rev.* 53, 1333–1347. <https://doi.org/10.1016/j.rser.2015.09.030>.
- Ahmad, A.A., Din, A.T.M., Yahaya, N.K.E.M., Karim, J., Ahmad, M.A., 2020. Atenolol sequestration using activated carbon derived from gasified *Glyricidia sepium*. *Arab. J. Chem.* 13 (10), 7544–7557. <https://doi.org/10.1016/j.arabjc.2020.08.029>.
- Ahmad, A.A., Ahmad, M.A., Yahya, N.K.E.M., Mohd Din, A.T., Wan Yaakub, A.R., 2020. Honeycomb-like porous-activated carbon derived from gasification waste for malachite green adsorption: equilibrium, kinetic, thermodynamic and fixed-bed column analysis. *Desalin. Water Treat.* 196, 329–347. <https://doi.org/10.5004/dwt.2020.26067>.
- Ahmad, A.A., Din, A.T.M., Yahaya, N.K.E.M., Khasri, A., Ahmad, M.A., 2020. Adsorption of basic green 4 onto gasified *Glyricidia sepium* woodchip based activated carbon: optimization, characterization, batch and column study. *Arab. J. Chem.* 13 (8), 6887–6903. <https://doi.org/10.1016/j.arabjc.2020.07.002>.
- Ahmad, N.N., Ahmad, A.A., Khasri, A., 2023. Effective removal of methylene blue from aqueous solution by adsorption onto gasification char: isotherm, kinetic and thermodynamics studies. *Desalin. Water Treat.* 285, 264–273. <https://doi.org/10.5004/dwt.2023.29274>.
- Ahmad, A.A., Ahmad, M.A., Yahaya, N.K.E.M., Karim, J., 2021. Adsorption of Malachite Green by Activated Carbon Derived from Gasified *Hevea brasiliensis* Root. *Arab. J. Chem.* 14, (4). <https://doi.org/10.1016/j.arabjc.2021.103104> 103104.
- Ahmed, M.J., Hameed, B.H., 2018. Adsorption behavior of salicylic acid on biochar as derived from the thermal pyrolysis of barley straws. *J. Clean. Prod.* 195, 1162–1169. <https://doi.org/10.1016/j.jclepro.2018.05.257>.
- Ahsan, M.A. et al., 2018. Adsorptive Removal of Sulfamethoxazole and Bisphenol A from Contaminated Water using Functionalized Carbonaceous Material Derived from Tea Leaves. *J. Environ. Chem. Eng.* 6 (4), 4215–4225. <https://doi.org/10.1016/j.jece.2018.06.022>.
- Albadarin, A.B., Solomon, S., Daher, M.A., Walker, G., 2018. Efficient removal of anionic and cationic dyes from aqueous systems using spent Yerba Mate 'Ilex paraguariensis'. *J. Taiwan Inst. Chem. Eng.* 82, 144–155. <https://doi.org/10.1016/j.jtice.2017.11.012>.
- Ali, M.M.M., Ahmed, M.J., Hameed, B.H., 2018. NaY zeolite from wheat (*Triticum aestivum* L.) straw ash used for the adsorption of tetracycline. *J. Clean. Prod.* 172, 602–608. <https://doi.org/10.1016/j.jclepro.2017.10.180>.
- Aljeboree, A.M., Alshirifi, A.N., Alkaim, A.F., 2017. Kinetics and equilibrium study for the adsorption of textile dyes on coconut shell activated carbon. *Arab. J. Chem.* 10, S3381–S3393.
- Al-zareer, M., Dincer, I., Rosen, M.A., 2016. Effects of various gasification parameters and operating conditions on syngas and hydrogen production. *Chem. Eng. Res. Des.* 115, 1–18. <https://doi.org/10.1016/j.cherd.2016.09.009>.
- Avrami, M., 1939. Kinetics of Phase Change. I General Theory. *J. Chem. Phys.* 7 (12), 1103–1112. <https://doi.org/10.1063/1.1750380>.
- Aworn, A., Thiravetyan, P., Nakbanpote, W., 2008. Preparation and characteristics of agricultural waste activated carbon by physical activation having micro- and mesopores. *J. Anal. Appl. Pyrolysis* 82, 279–285. <https://doi.org/10.1016/j.jaap.2008.04.007>.
- Ayawei, N., Ebelegi, A.N., Wankasi, D., 2017. Modelling and Interpretation of Adsorption Isotherms. *J. Chem.* 2017 (September), 1–11. <https://doi.org/10.1155/2017/3039817>.
- Azari, A., Yeganeh, M., Gholami, M., Salari, M., 2021. The superior adsorption capacity of 2,4-Dinitrophenol under ultrasound-assisted magnetic adsorption system: Modeling and process optimization by central composite design. *J. Hazard. Mater.* vol. 418, no. June., <https://doi.org/10.1016/j.jhazmat.2021.126348> 126348.
- Back, J.O., Hupfau, B., Rößler, A., Penner, S., Rupprich, M., 2020. Adsorptive removal of micropollutants from wastewater with floating-fixed-bed gasification char. *J. Environ. Chem. Eng.* 8 (3), pp. <https://doi.org/10.1016/j.jece.2020.103757>.
- Banerjee, S., Sharma, G.C., Gautam, R.K., Chattopadhyaya, M.C., Upadhyay, S.N., Sharma, Y.C., 2016. Removal of Malachite Green, a hazardous dye from aqueous solutions using *Avena sativa* (oat) hull as a potential adsorbent. *J. Mol. Liq.* 213, 162–172. <https://doi.org/10.1016/j.molliq.2015.11.011>.
- Bedia, J., Bolver, C., Ponce, S., Rodriguez, J.J.J., 2018. Adsorption of antipyrine by activated carbons from FeCl₃-activation of Tara gum. *Chem. Eng. J.* 333 (August 2017), 58–65. <https://doi.org/10.1016/j.cej.2017.09.161>.
- Behloul, H. et al., 2022. New insights on the adsorption of CI-Reactive Red 141 dye using activated carbon prepared from the ZnCl₂-treated waste cotton fibers: statistical physics, DFT, COSMO-RS, and AIM studies. *J. Mol. Liq.* 364., <https://doi.org/10.1016/j.molliq.2022.119956> 119956.
- Benedetti, V., Patuzzi, F., Baratieri, M., 2017. Characterization of char from biomass gasification and its similarities with activated carbon in adsorption applications. *Appl. Energy* 227, 92–99. <https://doi.org/10.1016/j.apenergy.2017.08.076>.
- Benedetti, V., Ail, S.S., Patuzzi, F., Baratieri, M., 2019. Valorization of char from biomass gasification as catalyst support in dry reforming of methane. *Front. Chem.* 7 (119), 1–12. <https://doi.org/10.3389/fchem.2019.00119>.
- Bhandari, P.N., Kumar, A., Bellmer, D.D., Huhnke, R.L., 2014. Synthesis and evaluation of biochar-derived catalysts for removal of toluene (model tar) from biomass-generated producer gas. *Renew. Energy* 66, 346–353. <https://doi.org/10.1016/j.renene.2013.12.017>.
- Bhattacharyya, R., Ray, S.K., 2015. Removal of congo red and methyl violet from water using nano clay filled composite hydrogels of poly acrylic acid and polyethylene glycol. *Chem. Eng. J.* 260, 269–283. <https://doi.org/10.1016/j.cej.2014.08.030>.
- Bohli, T., Nuria, F., Villaescusa, I., Ouederni, A., 2013. Adsorption on activated carbon from olive stones: kinetics and equilibrium of

- phenol removal from aqueous solution. *J. Chem. Eng. Process Technol.* 04 (06), pp. <https://doi.org/10.4172/2157-7048.1000165>.
- Bouaziz, F., Koubaa, M., Kallel, F., Ghorbel, R.E., Chaabouni, S.E., 2017. Adsorptive removal of malachite green from aqueous solutions by almond gum: kinetic study and equilibrium isotherms. *Int. J. Biol. Macromol.* 105, 56–65. <https://doi.org/10.1016/j.ijbiomac.2017.06.106>.
- Campos, N.F., Sales, D.C.S., Rodríguez-Díaz, J.M., Barbosa, C.M. B.M., Duarte, M.M.M.B., 2022. Adsorption of naphthenic acids on peanut shell activated carbon: Batch and fixed-bed column study of the process. *Chem. Eng. Res. Des.* 188, 633–644. <https://doi.org/10.1016/j.cherd.2022.10.023>.
- Chang, P.H., Jiang, W.T., Sarkar, B., Wang, W., Li, Z., 2019. The triple mechanisms of atenolol adsorption on Ca-montmorillonite: Implication in pharmaceutical wastewater treatment. *Materials (Basel)* 12 (18), pp. <https://doi.org/10.3390/ma12182858>.
- Cheah, S., Malone, S.C., Feik, C.J., 2014. Speciation of sulfur in biochar produced from pyrolysis and gasification of oak and corn stover. *Environ. Sci. Technol.* 48 (15), 8474–8480. <https://doi.org/10.1021/es500073r>.
- Chen, X. et al, 2022. Isotherm models for adsorption of heavy metals from water - A review. *Chemosphere* 307, (P1). <https://doi.org/10.1016/j.chemosphere.2022.135545> 135545.
- Cheng, N. et al, 2021. Adsorption of emerging contaminants from water and wastewater by modified biochar: A review. *Environ. Pollut.* 273,. <https://doi.org/10.1016/j.envpol.2021.116448> 116448.
- Choudhary, M., Kumar, R., Neogi, S., 2020. Activated biochar derived from *Opuntia ficus-indica* for the efficient adsorption of malachite green dye, Cu^{+2} and Ni^{+2} from water. *J. Hazard. Mater.* (February) <https://doi.org/10.1016/j.jhazmat.2020.122441> 122441.
- Chowdhury, S., Mishra, R., Saha, P., Kushwaha, P., 2011. Adsorption thermodynamics, kinetics and isosteric heat of adsorption of malachite green onto chemically modified rice husk. *Desalination* 265 (1–3), 159–168. <https://doi.org/10.1016/j.desal.2010.07.047>.
- Dai, L. et al, 2018. Calcium-rich biochar from crab shell: An unexpected super adsorbent for dye removal. *Bioresour. Technol.* 267, 510–516. <https://doi.org/10.1016/j.biortech.2018.07.090>.
- Danish, M., Ahmad, T., 2018. A review on utilization of wood biomass as a sustainable precursor for activated carbon production and application. *Renew. Sustain. Energy Rev.* 87, 1–21. <https://doi.org/10.1016/j.rser.2018.02.003>.
- De Gisi, S., Lofrano, G., Grassi, M., Notarnicola, M., 2016. Characteristics and adsorption capacities of low-cost sorbents for wastewater treatment: a review. *Sustain. Mater. Technol.* 9, 10–40. <https://doi.org/10.1016/j.susmat.2016.06.002>.
- Dias, D. et al, 2017. Properties of chars from the gasification and pyrolysis of rice waste streams towards their valorisation as adsorbent materials. *Waste Manag.* 65, 186–194. <https://doi.org/10.1016/j.wasman.2017.04.011>.
- Dias, D. et al, 2018. Cr(III) removal from synthetic and industrial wastewaters by using co-gasification chars of rice waste streams. *Bioresour. Technol.* 266 (April), 139–150. <https://doi.org/10.1016/j.biortech.2018.06.054>.
- Duan, X., Srinivasakannan, C., Wang, X., Wang, F., Liu, X., 2017. Synthesis of activated carbon fibers from cotton by microwave induced H_3PO_4 activation. *J. Taiwan Inst. Chem. Eng.* 70, 374–381. <https://doi.org/10.1016/j.jtice.2016.10.036>.
- Ducouso, M., Weiss-Hortala, E., Nzihou, A., Castaldi, M.J., 2015. Reactivity enhancement of gasification biochars for catalytic applications. *Fuel* 159, 491–499. <https://doi.org/10.1016/j.fuel.2015.06.100>.
- Ebadi, A., Soltan Mohammadzadeh, J.S., Khudiev, A., 2009. What is the correct form of BET isotherm for modeling liquid phase adsorption? *Adsorption* 15 (1), 65–73. <https://doi.org/10.1007/s10450-009-9151-3>.
- Fadhil, A.B., Ahmed, A.I., Salih, H.A., 2017. Production of liquid fuels and activated carbons from fish waste. *Fuel* 187, 435–445. <https://doi.org/10.1016/j.fuel.2016.09.064>.
- Feng, Z., Odelius, K., Rajarao, G.K., Hakkarainen, M., 2018. Microwave carbonized cellulose for trace pharmaceutical adsorption. *Chem. Eng. J.* 346 (April), 557–566. <https://doi.org/10.1016/j.cej.2018.04.014>.
- Ferkous, H. et al, 2022. The Removal of a Textile Dye from an Aqueous Solution Using a Biocomposite Adsorbent. *Polymers (Basel)* 14 (12), 1–15. <https://doi.org/10.3390/polym14122396>.
- Freundlich, H.M.F., 1906. Over the Adsorption in Solution. *J. Phys. Chem.* 57, 385–471.
- Fritz, W., Schluender, E.U., 1974. Simultaneous adsorption equilibria of organic solutes in dilute aqueous solutions on activated carbon. *Chem. Eng. Sci.* 29 (5), 1279–1282. [https://doi.org/10.1016/0009-2509\(74\)80128-4](https://doi.org/10.1016/0009-2509(74)80128-4).
- Fu, K., Yue, Q., Gao, B., Wang, Y., Li, Q., 2017. Activated carbon from tomato stem by chemical activation with FeCl_2 . *Colloids Surf. A* 529 (June), 842–849. <https://doi.org/10.1016/j.colsurfa.2017.06.064>.
- Fu, C., Zhang, H., Xia, M., Lei, W., Wang, F., 2020. The single co-adsorption characteristics and microscopic adsorption mechanism of biochar-montmorillonite composite adsorbent for pharmaceutical emerging organic contaminant atenolol and lead ions. *Ecotoxicol. Environ. Saf.* 187,. <https://doi.org/10.1016/j.ecoenv.2019.109763> 109763.
- Galhetas, M., Mestre, A.S., Pinto, M.L., Gulyurtlu, I., Lopes, H., Carvalho, A.P., 2014. Carbon-based materials prepared from pine gasification residues for acetaminophen adsorption. *Chem. Eng. J.* 240, 344–351. <https://doi.org/10.1016/j.cej.2013.11.067>.
- Galhetas, M., Mestre, A.S., Pinto, M.L., Gulyurtlu, I., Lopes, H., Carvalho, A.P., 2014. Chars from gasification of coal and pine activated with K_2CO_3 : acetaminophen and caffeine adsorption from aqueous solutions. *J. Colloid Interface Sci.* 433, 94–103.
- Galindo Al, C.V., Lora, E.S., Andrade, R.V., Giraldo, S.Y., Jaén, R. L., 2014. Biomass gasification in a downdraft gasifier with a two-stage air supply: effect of operating conditions on gas quality. *Biomass Bioenergy* 61, 236–244.
- Geçgel, Ü., Üner, O., Gökara, G., Bayrak, Y., 2016. Adsorption of cationic dyes on activated carbon obtained from waste *Elaeagnus* stone. *Adsorpt. Sci. Technol.* 34 (9–10), 512–525. <https://doi.org/10.1177/02636174166669727>.
- Godinho, D., Dias, D., Bernardo, M., Lapa, N., Fonseca, I., Lopes, H., Pinto, F., 2017. Adding value to gasification and co-pyrolysis chars as removal agents of Cr^{3+} . *J. Hazard. Mater.* 321, 173–182. <https://doi.org/10.1016/j.jhazmat.2016.09.006>.
- Gokce, Y., Aktas, Z., 2014. Nitric acid modification of activated carbon produced from waste tea and adsorption of methylene blue and phenol. *Appl. Surf. Sci.* 313, 352–359. <https://doi.org/10.1016/j.apsusc.2014.05.214>.
- Gong, Y. et al, 2019. p – p interaction effect in insertion polymerization with a -Diimine palladium systems. *J. Catal.* 378, 184–191. <https://doi.org/10.1016/j.jcat.2019.08.034>.
- Graham, D., 1953. The Characterization of Physical Adsorption Systems. I. The Equilibrium Function and Standard Free Energy of Adsorption. *J. Phys. Chem.* 57 (7), 665–669. <https://doi.org/10.1021/j150508a014>.
- Gupta, V.K., Gupta, B., Rastogi, A., Agarwal, S., Nayak, A., 2011. Pesticides removal from waste water by activated carbon prepared from waste rubber tire. *Water Res.* 45 (13), 4047–4055. <https://doi.org/10.1016/j.watres.2011.05.016>.
- Hadi, P., Xu, M., Ning, C., Sze Ki Lin, C., McKay, G., 2015. A critical review on preparation, characterization and utilization of sludge-derived activated carbons for wastewater treatment. *Chem. Eng. J.* 260, 895–906. <https://doi.org/10.1016/j.cej.2014.08.088>.
- Hansen, V., Müller-Stöver, D., Ahrenfeldt, J., Holm, J.K., Henriksen, U.B., Hauggaard-Nielsen, H., 2015. Gasification biochar as a valuable by-product for carbon sequestration and soil amendment. *Biomass and Bioenergy* 72 (1), 300–308. <https://doi.org/10.1016/j.biombioe.2014.10.013>.

- Haro, N.K., Del Vecchio, P., Marcilio, N.R., F eris, L.A., 2017. Removal of atenolol by adsorption – Study of kinetics and equilibrium. *J. Clean. Prod.* 154, 214–219. <https://doi.org/10.1016/j.jclepro.2017.03.217>.
- Hern andez, J.J., Lapuerta, M., Monedero, E., 2016. Characterisation of residual char from biomass gasification: effect of the gasifier operating conditions. *J. Clean. Prod.* <https://doi.org/10.1016/j.jclepro.2016.05.120>.
- Ho, Y.S., McKay, G., 1999. Pseudo-second order model for sorption. pdf. *Process Biochem.* 34, 451–465.
- Horv ath, K., Vajda, P., Felinger, A., 2017. Multilayer adsorption in liquid chromatography – The surface heterogeneity below an adsorbed multilayer. *J. Chromatogr. A* 1505, 50–55. <https://doi.org/10.1016/j.chroma.2017.05.020>.
- Huang, W., Wu, R., Chang, J., Juang, S., Lee, D., 2023. Bioresource Technology Manganese ferrite modified agricultural waste-derived biochars for copper ions adsorption. *Bioresour. Technol.* 367 (October 2022). <https://doi.org/10.1016/j.biortech.2022.128303>.
- Huggins, T.M., Pietron, J.J., Wang, H., Jason, Z., Biffinger, J.C., 2015. Graphitic biochar as a cathode electrocatalyst support for microbial fuel cells. *Bioresour. Technol.* 195, 147–153. <https://doi.org/10.1016/j.biortech.2015.06.012>.
- Ibrahim, W.M., Hassan, A.F., Azab, Y.A., 2016. Biosorption of toxic heavy metals from aqueous solution by *Ulva lactuca* activated carbon. *Egypt. J. Basic Appl. Sci.* 3 (3), 241–249. <https://doi.org/10.1016/j.ejbas.2016.07.005>.
- IMARC Group, Biomass Gasification Market: Global Industry Trends, Share, Size, Growth, Opportunity and Forecast 2018-2023, *IMARC Group, United States*, 2017. <https://www.researchandmarkets.com/reports/4535020/biomass-gasification-market-global-industry>.
- Ippolito, J.A. et al, 2020. Feedstock choice, pyrolysis temperature and type influence biochar characteristics: a comprehensive meta-data analysis review. *Biochar* 2 (4), 421–438. <https://doi.org/10.1007/s42773-020-00067-x>.
- Jain, S.N., Gogate, P.R., 2018. Efficient removal of Acid Green 25 dye from wastewater using activated *Prunus Dulcis* as biosorbent: Batch and column studies. *J. Environ. Manage.* 210, 226–238. <https://doi.org/10.1016/j.jenvman.2018.01.008>.
- Jang, H.M., Kan, E., 2019. A novel hay-derived biochar for removal of tetracyclines in water. *Bioresour. Technol.* 274 (October 2018), 162–172. <https://doi.org/10.1016/j.biortech.2018.11.081>.
- Jung, H., Sewu, D.D., Ohemeng-Boahen, G., Lee, D.S., Woo, S.H., 2019. Characterization and adsorption performance evaluation of waste char by-product from industrial gasification of solid refuse fuel from municipal solid waste. *Waste Manage.* 91, 33–41. <https://doi.org/10.1016/j.wasman.2019.04.053>.
- Kallel, F., Chaari, F., Bouaziz, F., Bettaieb, F., Ghorbel, R., Chaabouni, S.E., 2016. Sorption and desorption characteristics for the removal of a toxic dye, methylene blue from aqueous solution by a low cost agricultural by-product. *J. Mol. Liq.* 219, 279–288. <https://doi.org/10.1016/j.molliq.2016.03.024>.
- Karthikeyan, S., Sivakumar, B., Sivakumar, N., 2010. Film and pore diffusion modeling for adsorption of reactive red 2 from aqueous solution on to activated carbon prepared from bio-diesel industrial waste. *E-Journal Chem.* 7 (SUPPL. 1), 175–185. <https://doi.org/10.1155/2010/138684>.
- Kasperiski, F.M. et al, 2018. Production of porous activated carbons from *Caesalpinia ferrea* seed pod wastes : Highly efficient removal of captopril from aqueous solutions. *J. Clean. Prod.* 197, 919–929. <https://doi.org/10.1016/j.jclepro.2018.06.146>.
- Khasri, A., Bello, O.S., Ahmad, M.A., 2018. Mesoporous activated carbon from Pentace species sawdust via microwave-induced KOH activation: optimization and methylene blue adsorption. *Res. Chem. Intermed.* 44 (May), 1–21. <https://doi.org/10.1007/s11164-018-3452-7>.
- Khasri, A., Jamir, M.R.M., Ahmad, A.A., Ahmad, M.A., 2021. Adsorption of remazol brilliant violet 5r dye from aqueous solution onto melunak and rubberwood sawdust based activated carbon: Interaction mechanism, isotherm, kinetic and thermodynamic properties. *Desalin. Water Treat.* 216, 401–411. <https://doi.org/10.5004/dwt.2021.26852>.
- Kilpimaa, S., Runtti, H., Kangas, T., Lassi, U., Kuokkanen, T., 2014. Removal of phosphate and nitrate over a modified carbon residue from biomass gasification. *Chem. Eng. Res. Des.* 92 (10), 1923–1933. <https://doi.org/10.1016/j.cherd.2014.03.019>.
- Kilpimaa, S., Runtti, H., Kangas, T., Lassi, U., Kuokkanen, T., 2015. Physical activation of carbon residue from biomass gasification : Novel sorbent for the removal of phosphates and nitrates from aqueous solution. *J. Ind. Eng. Chem.* 21, 1354–1364. <https://doi.org/10.1016/j.jiec.2014.06.006>.
- Klasson, K.T., Wartelle, L.H., Rodgers, J.E., Lima, I.M., 2009. Copper(II) adsorption by activated carbons from pecan shells: Effect of oxygen level during activation. *Ind. Crops Prod.* 30 (1), 72–77. <https://doi.org/10.1016/j.indcrop.2009.01.007>.
- Kutluay, S., Baytar, O., Şahin,  ., 2019. Equilibrium, kinetic and thermodynamic studies for dynamic adsorption of benzene in gas phase onto activated carbon produced from *elaegnus angustifolia* seeds. *J. Environ. Chem. Eng.* 7, <https://doi.org/10.1016/j.jece.2019.102947> 102947.
- Kwon, S., Fan, M., DaCosta, H.F.M., Russell, A.G., Berchtold, K. A., Dubey, M.K., 2011 Chapter 10. In: *CO₂ Sorption*. William Andrew Publishing, Boston, pp. 293–339.
- Lagergren, S.K., 1898. About the theory of so-called adsorption of soluble substances. *Sven. Vetenskapsakad. Handlingar* 24, 1–39 <https://ci.nii.ac.jp/naid/10016440244/en/>.
- Laksaci, H., Kheli, A., Belhamdi, B., Trari, M., 2017. Valorization of coffee grounds into activated carbon using physic — chemical activation by KOH/CO₂. *J. Environ. Chem. Eng.* 5 (September), 5061–5066. <https://doi.org/10.1016/j.jece.2017.09.036>.
- Langley, L.A., Fairbrother, D.H., 2007. Effect of wet chemical treatments on the distribution of surface oxides on carbonaceous materials. *Carbon N. Y.* 45 (1), 47–54. <https://doi.org/10.1016/j.carbon.2006.08.008>.
- Langmuir, I., 1918. The adsorption of gases on plane surfaces of glass, mica and platinum. *J. Am. Chem. Soc.* 40 (9), 1361–1403. <https://doi.org/10.1021/ja02242a004>.
- Li, N. et al, 2022. Municipal solid waste derived biochars for wastewater treatment: Production, properties and applications. *Resour. Conserv. Recycl.* 177, (135). <https://doi.org/10.1016/j.resconrec.2021.106003> 106003.
- Liu, C. et al, 2018. Influences of equivalence ratio, oxygen concentration and fluidization velocity on the characteristics of oxygen-enriched gasification products from biomass in a pilot-scale fluidized bed. *Int. J. Hydrogen Energy* 43 (31), 14214–14225. <https://doi.org/10.1016/j.ijhydene.2018.05.154>.
- Liu, M. et al, 2021. Char reactivity and kinetics based on the dynamic char structure during gasification by CO₂. *Fuel Process. Technol.* 211 (June 2020). <https://doi.org/10.1016/j.fuproc.2020.106583>.
- Liu, P., Liu, W.J., Jiang, H., Chen, J.J., Li, W.W., Yu, H.Q., 2012. Modification of bio-char derived from fast pyrolysis of biomass and its application in removal of tetracycline from aqueous solution. *Bioresour. Technol.* 121, 235–240. <https://doi.org/10.1016/j.biortech.2012.06.085>.
- Low, M.J.D., Jun. 1960. Kinetics of Chemisorption of Gases on Solids. *Chem. Rev.* 60 (3), 267–312. <https://doi.org/10.1021/cr60205a003>.
- Low, S.K., Tan, M.C., 2018. Dye adsorption characteristic of ultrasound pre-treated pomelo peel. *J. Environ. Chem. Eng.* 6 (2), 3502–3509. <https://doi.org/10.1016/j.jece.2018.05.013>.
- Lundberg, L., Tchoffor, P.A., Pallar es, D., Johansson, R., Thunman, H., Davidsson, K., 2016. Influence of surrounding conditions and fuel size on the gasification rate of biomass char in a fluidized bed. *Fuel Process. Technol.* 144, 323–333. <https://doi.org/10.1016/j.fuproc.2016.01.002>.

- Maia, G.S., de Andrade, J.R., da Silva, M.G.C., Vieira, M.G.A., 2019. Adsorption of diclofenac sodium onto commercial organo-clay: Kinetic, equilibrium and thermodynamic study. *Powder Technol.* 345, 140–150. <https://doi.org/10.1016/j.powtec.2018.12.097>.
- Maneerung, T., Liew, J., Dai, Y., Kawi, S., Chong, C., Wang, C.H., 2016. Activated carbon derived from carbon residue from biomass gasification and its application for dye adsorption: kinetics, isotherms and thermodynamic studies. *Bioresour. Technol.* 200, 350–359. <https://doi.org/10.1016/j.biortech.2015.10.047>.
- Marks, E.A.N., Mattana, S., Alcañiz, J.M., Pérez-herrero, E., Domene, X., 2016. Gasifier biochar effects on nutrient availability, organic matter mineralization, and soil fauna activity in a multi-year Mediterranean trial. *Agric. Ecosyst. Environ.* 215, 30–39. <https://doi.org/10.1016/j.agee.2015.09.004>.
- Marsh, H., Rodríguez-Reinoso, F., 2006. Porosity in Carbons: Modeling, in *Activated Carbon*. Elsevier, Oxford, pp. 87–142.
- Mohebalı, S., Bastani, D., Shayesteh, H., 2019. Equilibrium, kinetic and thermodynamic studies of a low-cost biosorbent for the removal of Congo red dye: acid and CTAB-acid modified celery (*Apium graveolens*). *J. Mol. Struct.* 1176, 181–193. <https://doi.org/10.1016/j.molstruc.2018.08.068>.
- Morali, U., Demiral, H., Şensöz, S., 2018. Optimization of activated carbon production from sunflower seed extracted meal: Taguchi design of experiment approach and analysis of variance. *J. Clean. Prod.* 189, 602–611. <https://doi.org/10.1016/j.jclepro.2018.04.084>.
- Nam, H., Choi, W., Genuino, D.A., Capareda, S.C., 2018. Development of rice straw activated carbon and its utilizations. *J. Environ. Chem. Eng.* 6 (4), 5221–5229. <https://doi.org/10.1016/j.jece.2018.07.045>.
- Nguyen, H., You, S., Hosseini-bandegharai, A., Chao, H.-P., 2017. Mistakes and inconsistencies regarding adsorption of contaminants from aqueous solutions: a critical review. *Water Res.* 120, 88–116. <https://doi.org/10.1016/j.watres.2017.04.014>.
- Ogata, F., Tominaga, H., Kangawa, M., Kawasaki, N., 2011. Adsorption of Cadmium Ions by Wheat Bran Treated with Pectinase. *Chem. Pharm. Bull. (Tokyo)* 59 (11), 1400–1402. <https://doi.org/10.1248/cpb.59.1400>.
- Ogata, F., Nakamura, T., Kawasaki, N., 2018. Adsorption capability of virgin and calcined wheat bran for molybdenum present in aqueous solution and elucidating the adsorption mechanism by adsorption isotherms, kinetics, and regeneration. *J. Environ. Chem. Eng.* 6 (4), 4459–4466. <https://doi.org/10.1016/j.jece.2018.06.047>.
- Ogunbenro, A.E., Quang, D.V., Al-Ali, K.A., Vega, L.F., Abu-Zahra, M.R.M., 2018. Physical synthesis and characterization of activated carbon from date seeds for CO₂ capture. *J. Environ. Chem. Eng.* 6 (4), 4245–4252. <https://doi.org/10.1016/j.jece.2018.06.030>.
- Oni, B.A., Oziegbe, O., Olawole, O.O., 2019. Significance of biochar application to the environment and economy. *Ann. Agric. Sci.* 64 (2), 222–236. <https://doi.org/10.1016/j.aas.2019.12.006>.
- Oyelude, E.O., Awudza, J.A.M., Twumasi, S.K., 2018. Removal of malachite green from aqueous solution using pulverized teak leaf litter: equilibrium, kinetic and thermodynamic studies. *Chem. Cent. J.* 12 (1), 1–10. <https://doi.org/10.1186/s13065-018-0448-8>.
- Palies, P., 2020. “2 - Premixed combustion for combustors. In: Stabilization and Dynamic of Premixed Swirling Flames: Prevariorized, Stratified, Partially, and Fully Premixed Regimes, P. B. T.-S. and D. of P. S. F. Palies, Ed. Academic Press, pp. 57–103.
- Pallarés, J., González-cencerrado, A., Arauzo, I., 2018. Production and characterization of activated carbon from barley straw by physical activation with carbon dioxide and steam. *Biomass and Bioenergy* 115 (January), 64–73. <https://doi.org/10.1016/j.biombioe.2018.04.015>.
- Pap, S., Šolević Knudsen, T., Radonić, J., Maletić, S., Igić, S.M., Turk Sekulić, M., 2017. Utilization of fruit processing industry waste as green activated carbon for the treatment of heavy metals and chlorophenols contaminated water. *J. Clean. Prod.* 162, 958–972. <https://doi.org/10.1016/j.jclepro.2017.06.083>.
- Pelaez-samaniego, M.R., Perez, J.F., Ayiania, M., Garcia-perez, T., 2020. Chars from wood gasification for removing H₂S from biogas. *Biomass and Bioenergy* 142, (September). <https://doi.org/10.1016/j.biombioe.2020.105754> 105754.
- Pereira, M., Henrique, P., Chaves, E., Dotto, G.L., Kessler, F., Grasel, F.S., 2018. Preparation of an alternative adsorbent from *Acacia Mearnsii* wastes through acetosolv method and its application for dye removal. *J. Cleaner Product.* 180, 386–394.
- Pessôa, T.S. et al, 2019. Açai waste benefiting by gasification process and its employment in the treatment of synthetic and raw textile wastewater. *J. Clean. Prod.* 240. <https://doi.org/10.1016/j.jclepro.2019.118047>.
- Popoola, L.T., Yusuff, A.S., Adesina, O.A., Lala, M.A., 2019. Brilliant Green Dye Sorption onto Snail Shell-rice Husk: Statistical and Error Function Models as Parametric Isotherm Predictors. *J. Environ. Sci. Technol.* 12 (2), 65–80. <https://doi.org/10.3923/jest.2019.65.80>.
- Prauchner, M.J., Rodríguez-Reinoso, F., 2012. Chemical versus physical activation of coconut shell: a comparative study. *Micro-porous Mesoporous Mater.* 152, 163–171. <https://doi.org/10.1016/j.micromeso.2011.11.040>.
- Qian, K. et al, 2013. Effects of biomass feedstocks and gasification conditions on the physicochemical properties of char. *Energies* 6 (8), 3972–3986. <https://doi.org/10.3390/en6083972>.
- Qian, K., Kumar, A., Bellmer, D., Yuan, W., Wang, D., Eastman, M. A., 2015. Physical properties and reactivity of char obtained from downdraft gasification of sorghum and eastern red cedar. *Fuel* 143, 383–389. <https://doi.org/10.1016/j.fuel.2014.11.054>.
- Qu, W., Yuan, T., Yin, G., Xu, S., Zhang, Q., Su, H., 2019. Effect of properties of activated carbon on malachite green adsorption. *Fuel* 249 (October 2018), 45–53. <https://doi.org/10.1016/j.fuel.2019.03.058>.
- Rajapaksha, A.U. et al, 2016. Engineered/designer biochar for contaminant removal/immobilization from soil and water: potential and implication of biochar modification. *Chemosphere* 148, 276–291. <https://doi.org/10.1016/j.chemosphere.2016.01.043>.
- Rangabhashiyam, S., Lata, S., Balasubramanian, P., 2018. Biosorption characteristics of methylene blue and malachite green from simulated wastewater onto *Carica papaya* wood biosorbent. *Surf. Interfaces* 10 (September 2017), 197–215. <https://doi.org/10.1016/j.surfin.2017.09.011>.
- Rashidi, N.A., Yusup, S., 2017. A review on recent technological advancement in the activated carbon production from oil palm wastes. *Chem. Eng. J.* 314, 277–290. <https://doi.org/10.1016/j.cej.2016.11.059>.
- Rashtbari, Y., Hazrati, S., Azari, A., Afshin, S., Fazlzadeh, M., Vosoughi, M., 2020. A novel, eco-friendly and green synthesis of PPAC-ZnO and PPAC-nZVI nanocomposite using pomegranate peel: Cephalexin adsorption experiments, mechanisms, isotherms and kinetics. *Adv. Powder Technol.* 31 (4), 1612–1623. <https://doi.org/10.1016/j.apt.2020.02.001>.
- Rathi, B.S., Kumar, P.S., 2021. Application of adsorption process for effective removal of emerging contaminants from water and wastewater. *Environ. Pollut.* 280,. <https://doi.org/10.1016/j.envpol.2021.116995> 116995.
- Ravenni, G., Sárossy, Z., Sanna, S., Ahrenfeldt, J., Henriksen, U.B., 2020. Residual gasification char applied to tar reforming in a pilot-scale gasifier: Performance and evolution of char properties for perspective cascade uses. *Fuel Process. Technol.* 210, (April). <https://doi.org/10.1016/j.fuproc.2020.106546> 106546.
- Ravenni, G., Cafaggi, G., Sárossy, Z., Rohde Nielsen, K.T., Ahrenfeldt, J., Henriksen, U.B., 2020. Waste chars from wood gasification and wastewater sludge pyrolysis compared to commercial activated carbon for the removal of cationic and anionic dyes from aqueous solution. *Bioresour. Technol. Rep.* 10, (March). <https://doi.org/10.1016/j.biteb.2020.100421> 100421.

- Reffas, A. et al, 2010. Carbons prepared from coffee grounds by H_3PO_4 activation: characterization and adsorption of methylene blue and Nylosan Red N-2RBL. *J. Hazard. Mater.* 175 (1–3), 779–788. <https://doi.org/10.1016/j.jhazmat.2009.10.076>.
- Ribas, M.C. et al, 2014. Comparison of a homemade cocoa shell activated carbon for reactive violet 5 dye. *Chem. Eng. J.* 248, 315–326.
- Rivera-Utrilla, J., Sánchez-Polo, M., Gómez-Serrano, V., Álvarez, P. M., Alvim-Ferraz, M.C.M., Dias, J.M., 2011. Activated carbon modifications to enhance its water treatment applications. An overview. *J. Hazard. Mater.* 187 (1–3), 1–23. <https://doi.org/10.1016/j.jhazmat.2011.01.033>.
- Rodrigues, L.A., Caetano Pinto da Silva, M.L., Alvarez-Mendes, M. O., Coutinho, A.d.R., PatrocínioThim, G., 2011. Phenol removal by activated carbon produced from avocado kernel seeds. *Chem. Eng. J.* 174, 49–57.
- Rouibah, K. et al, Jan. 2023. Biosorption of zinc (II) from synthetic wastewater by using *Inula Viscosa* leaves as a low-cost biosorbent: Experimental and molecular modeling studies. *J. Environ. Manage.* 326,. <https://doi.org/10.1016/j.jenvman.2022.116742> 116742.
- Runtti, H., Tuomikoski, S., Kangas, T., Lassi, U., Kuokkanen, T., Rämö, J., 2014. Chemically activated carbon residue from biomass gasification as a sorbent for iron(II), copper(II) and nickel(II) ions. *J. Water Process Eng.* 4, 12–24. <https://doi.org/10.1016/j.jwpe.2014.08.009>.
- Runtti, H., Tuomikoski, S., Kangas, T., Kuokkanen, T., Rämö, J., Lassi, U., 2016. Sulphate removal from water by carbon residue from biomass gasification: Effect of chemical modification methods on sulphate removal efficiency. *BioResources* 11 (2), 3136–3152. <https://doi.org/10.15376/biores.11.2.3136-3152>.
- Saadi, R., Saadi, Z., Fazaali, R., Fard, N.E., 2015. Monolayer and multilayer adsorption isotherm models for sorption from aqueous media. *Korean J. Chem. Eng.* 32 (5), 787–799. <https://doi.org/10.1007/s11814-015-0053-7>.
- Saffè, A., Collado, R., Monedero, E., 2020. Recirculation of char from biomass gasification: effects on gasifier performance and end-char properties. *Renew. Energy* 147, 806–813. <https://doi.org/10.1016/j.renene.2019.09.063>.
- Sajjadi, S.A. et al, 2018. Efficient mercury removal from wastewater by pistachio wood wastes-derived activated carbon prepared by chemical activation using a novel activating agent. *J. Environ. Manage.* 223 (July), 1001–1009. <https://doi.org/10.1016/j.jenvman.2018.06.077>.
- Sánchez-Polo, M., Rivera-Utrilla, J., 2002. Adsorbent - Adsorbate Interactions in the Adsorption of Cd (II) and Hg (II) on Ozonized Activated Carbons. *Environ. Sci. Technol.* 36 (17), 3850–3854.
- Saravanan, A., Kumar, P.S., Renita, A.A., 2018. Hybrid synthesis of novel material through acid modification followed ultrasonication to improve adsorption capacity for zinc removal. *J. Clean. Prod.* 172, 92–105. <https://doi.org/10.1016/j.jclepro.2017.10.109>.
- Saygili, H., Güzel, F., 2015. Performance of new mesoporous carbon sorbent prepared from grape industrial processing wastes for malachite green and congo red removal. *Chem. Eng. Res. Des.* 100, 27–38. <https://doi.org/10.1016/j.cherd.2015.05.014>.
- Schaeffer, K., Jun. 2011. Activated Carbon Market - Supply and Demand Update – Or The Carbon Conundrum. *Water Conditioning & Purification, Tucson, Arizona.*
- Scheufler, F.B. et al, 2016. Monolayer-multilayer adsorption phenomenological model: Kinetics, equilibrium and thermodynamics. *Chem. Eng. J.* 284, 1328–1341. <https://doi.org/10.1016/j.cej.2015.09.085>.
- Seredych, M., Lison, J., Jans, U., Badosz, T.J., 2009. Textural and chemical factors affecting adsorption capacity of activated carbon in highly efficient desulfurization of diesel fuel. *Carbon* N. Y. 47 (10), 2491–2500. <https://doi.org/10.1016/j.carbon.2009.05.001>.
- Sewu, D.D., Boakye, P., Woo, S.H., 2017. Highly efficient adsorption of cationic dye by biochar produced with Korean cabbage waste. *Bioresour. Technol.* 224, 206–213. <https://doi.org/10.1016/j.biortech.2016.11.009>.
- Shafeeyan, M.S., Daud, W.M.A.W., Houshmand, A., Shamiri, A., 2010. A review on surface modification of activated carbon for carbon dioxide adsorption. *J. Anal. Appl. Pyrolysis* 89 (2), 143–151. <https://doi.org/10.1016/j.jaap.2010.07.006>.
- Sharma, G. et al, 2019. Honeycomb structured activated carbon synthesized from *Pinus roxburghii* cone as effective bioadsorbent for toxic malachite green dye. *J. Water Process Eng.* vol. 32, no. August,. <https://doi.org/10.1016/j.jwpe.2019.100931> 100931.
- Shen, Y., Linville, J.L., Ignacio-de Leon, P.A.A., Schoene, R.P., Urgun-Demirtas, M., 2016. Towards a sustainable paradigm of waste-to-energy process: enhanced anaerobic digestion of sludge with woody biochar. *J. Clean. Prod.* 135, 1054–1064. <https://doi.org/10.1016/j.jclepro.2016.06.144>.
- Shoib, M., Al-swaidan, H.M., 2015. Optimization and characterization of sliced activated carbon prepared from date palm tree fronds by physical activation. *Biomass and Bioenergy* 73, 124–134. <https://doi.org/10.1016/j.biombioe.2014.12.016>.
- Shu, T., Lu, P., He, N., 2013. Mercury adsorption of modified mulberry twig chars in a simulated flue gas. *Bioresour. Technol.* 136, 182–187. <https://doi.org/10.1016/j.biortech.2013.02.087>.
- Singh, J., Bhunia, H., Basu, S., 2019. Adsorption of CO_2 on KOH activated carbon adsorbents: effect of different mass ratios. *J. Environ. Manage.* 250,. <https://doi.org/10.1016/j.jenvman.2019.109457> 109457.
- Şolpan, D., Duran, S., Saraydin, D., Güven, O., cedilolpan et al.. Adsorption of methyl violet in aqueous solutions by poly(acrylamide-co-acrylic acid) hydrogels. *Radiat. Phys. Chem.* 66 (2), 117–127. [https://doi.org/10.1016/S0969-806X\(02\)00384-5](https://doi.org/10.1016/S0969-806X(02)00384-5).
- Sophia, C.A., Lima, E.C., 2018. Removal of emerging contaminants from the environment by adsorption. *Ecotoxicol. Environ. Saf.* 150, 1–17. <https://doi.org/10.1016/j.ecoenv.2017.12.026>.
- Sotelo, J.L., Rodríguez, A.R., Mateos, M.M., Hernández, S.D., Silvia Torrellas, A., Rodríguez, J.G., 2012. Adsorption of pharmaceutical compounds and an endocrine disruptor from aqueous solutions by carbon materials. *J. Environ. Sci. Heal., Part B Pestic., Food Contam., Agric. Wastes* 47 (7), 640–652. <https://doi.org/10.1080/03601234.2012.668462>.
- Sotelo, J.L., Ovejero, G., Rodríguez, A., Álvarez, S., García, J., 2012. Removal of atenolol and isoproturon in aqueous solutions by adsorption in a fixed-bed column. *Ind. Eng. Chem. Res.* 51 (13), 5045–5055. <https://doi.org/10.1021/ie300334q>.
- Spagnoli, A.A., Giannakoudakis, D.A., Bashkova, S., 2017. Adsorption of methylene blue on cashew nut shell based carbons activated with zinc chloride: the role of surface and structural parameters. *J. Mol. Liquids* 229, 465–471. <https://doi.org/10.1016/j.molliq.2016.12.106>.
- Stavropoulos, G.G., Samaras, P., Sakellariopoulos, G.P., 2008. Effect of activated carbons modification on porosity, surface structure and phenol adsorption. *J. Hazard. Mater.* 151 (2–3), 414–421. <https://doi.org/10.1016/j.jhazmat.2007.06.005>.
- Sumalinog, D.A.G., Capareda, S.C., de Luna, M.D.G., 2018. Evaluation of the effectiveness and mechanisms of acetaminophen and methylene blue dye adsorption on activated biochar derived from municipal solid wastes. *J. Environ. Manage.* 210, 255–262. <https://doi.org/10.1016/j.jenvman.2018.01.010>.
- Sun, K., Jiang, J., 2010. Preparation and characterization of activated carbon from rubber-seed shell by physical activation with steam. *Biomass and Bioenergy* 34 (4), 539–544. <https://doi.org/10.1016/j.biombioe.2009.12.020>.
- Suo, F. et al, 2019. Mesoporous activated carbon from starch for superior rapid pesticides removal. *Int. J. Biol. Macromol.* 121, 806–813. <https://doi.org/10.1016/j.ijbiomac.2018.10.132>.
- Sy, L., Km, B., Arvind, K., 2017. Batch and column studies for phenol removal from aqueous solutions using laboratory prepared low-cost activated carbon as an adsorbent. *Chem. Technol. An Indian J.* 12 (2), 1–32.

- Tan, K.L., Hameed, B.H., 2017. Insight into the adsorption kinetics models for the removal of contaminants from aqueous solutions. *J. Taiwan Inst. Chem. Eng.* 74, 25–48. <https://doi.org/10.1016/j.jtice.2017.01.024>.
- Theydan, S.K., Ahmed, M.J., 2012. Adsorption of methylene blue onto biomass-based activated carbon by FeCl₃ activation: Equilibrium, kinetics, and thermodynamic studies. *J. Anal. Appl. Pyrolysis* 97, 116–122. <https://doi.org/10.1016/j.jaap.2012.05.008>.
- Thommes, M., 2010. Physical adsorption characterization of nanoporous materials. *Chemie-Ingenieur-Technik* 82 (7), 1059–1073. <https://doi.org/10.1002/cite.201000064>.
- Tian, H., Hu, Q., Wang, J., Liu, L., Yang, Y., Bridgwater, A.V., 2020. Steam gasification of *Miscanthus* derived char: the reaction kinetics and reactivity with correlation to the material composition and microstructure. *Energy Convers. Manag.* 219, (May). <https://doi.org/10.1016/j.enconman.2020.113026> 113026.
- To, M.H., Hadi, P., Hui, C.W., Lin, C.S.K., McKay, G., 2017. Mechanistic study of atenolol, acebutolol and carbamazepine adsorption on waste biomass derived activated carbon. *J. Mol. Liq.* 241, 386–398. <https://doi.org/10.1016/j.molliq.2017.05.037>.
- Toth, J., 1971. State equation of the solid-gas interface layers. *Acta chim. hung.* 69, 311–328.
- Toumi, K.H. et al, 2018. Molecular modeling of cationic dyes adsorption on agricultural Algerian olive cake waste. *J. Mol. Liq.* 264, 127–133. <https://doi.org/10.1016/j.molliq.2018.05.045>.
- Tounsadi, H. et al, 2016. Highly efficient activated carbon from *Glebionis coronaria* L. biomass: optimization of preparation conditions and heavy metals removal using experimental design approach. *J. Environ. Chem. Eng.* 4 (4), 4549–4564. <https://doi.org/10.1016/j.jece.2016.10.020>.
- Tran, H.N., Wang, Y.F., You, S.J., Chao, H.P., 2017. Insights into the mechanism of cationic dye adsorption on activated charcoal: The importance of π - π interactions. *Process Saf. Environ. Prot.* 107, 168–180. <https://doi.org/10.1016/j.psep.2017.02.010>.
- Trubetskaya, A., Kling, J., Ershag, O., Attard, T.M., Schröder, E., 2019. Removal of phenol and chlorine from wastewater using steam activated biomass soot and tire carbon black. *J. Hazard. Mater.* 365 (May 2018), 846–856. <https://doi.org/10.1016/j.jhazmat.2018.09.061>.
- Uchimiya, M., Chang, S., Klasson, K.T., 2011. Screening biochars for heavy metal retention in soil: Role of oxygen functional groups. *J. Hazard. Mater.* 190 (1–3), 432–441. <https://doi.org/10.1016/j.jhazmat.2011.03.063>.
- Ullah, F. et al, 2022. Adsorption performance and mechanism of cationic and anionic dyes by KOH activated biochar derived from medical waste pyrolysis. *Environ. Pollut.* 314, (September). <https://doi.org/10.1016/j.envpol.2022.120271> 120271.
- Wakkal, M., Khiari, B., Zagrouba, F., 2019. Textile wastewater treatment by agro-industrial waste: Equilibrium modelling, thermodynamics and mass transfer mechanisms of cationic dyes adsorption onto low-cost lignocellulosic adsorbent. *J. Taiwan Inst. Chem. Eng.* 96, 439–452. <https://doi.org/10.1016/j.jtice.2018.12.014>.
- Weber, K., Quicker, P., 2018. Properties of biochar. *Fuel* 217, 240–261. <https://doi.org/10.1016/j.fuel.2017.12.054>.
- Wiedner, K., Rumpel, C., Steiner, C., Pozzi, A., Maas, R., Glaser, B., 2013. Chemical evaluation of chars produced by thermochemical conversion (gasification, pyrolysis and hydrothermal carbonization) of agro-industrial biomass on a commercial scale. *Biomass and Bioenergy* 59, 264–278. <https://doi.org/10.1016/j.biombioe.2013.08.026>.
- Xu, R., Xiao, S., Yuan, J., Zhao, A., 2011. Adsorption of methyl violet from aqueous solutions by the biochars derived from crop residues. *Bioresour. Technol.* 102, 10293–10298. <https://doi.org/10.1016/j.biortech.2011.08.089>.
- Xue, Y. et al, 2012. Hydrogen peroxide modification enhances the ability of biochar (hydrochar) produced from hydrothermal carbonization of peanut hull to remove aqueous heavy metals: Batch and column tests. *Chem. Eng. J.* 200–202, 673–680.
- Yagub, M.T., Sen, T.K., Afroze, S., Ang, H.M., 2014. Dye and its removal from aqueous solution by adsorption: a review. *Adv. Colloid Interface Sci.* 209, 172–184. <https://doi.org/10.1016/j.cis.2014.04.002>.
- Yanan, C. et al, 2022. Adsorption of paracetamol and ketoprofen on activated charcoal prepared from the residue of the fruit of *Butiacapitate*: Experiments and theoretical interpretations. *Chem. Eng. J.* 454 (September), 2023. <https://doi.org/10.1016/j.cej.2022.139943>.
- You, S. et al, 2017. A critical review on sustainable biochar system through gasification: Energy and environmental applications. *Bioresour. Technol.* <https://doi.org/10.1016/j.biortech.2017.06.177>.
- Yu, D., Wang, L., Wu, M., 2018. Simultaneous removal of dye and heavy metal by banana peels derived hierarchically porous carbons. *J. Taiwan Inst. Chem. Eng.* 93, 543–553. <https://doi.org/10.1016/j.jtice.2018.08.038>.
- Yuan, C. et al, 2021. Steam gasification of char derived from penicillin mycelial dreg and lignocellulosic biomass: influence of P, K and Ca on char reactivity. *Energy*. <https://doi.org/10.1016/j.energy.2021.120605>.
- Zbair, M., Anfar, Z., Ahsaine, H.A., El Alem, N., Ezahri, M., 2018. Acridine orange adsorption by zinc oxide / almond shell activated carbon composite: operational factors, mechanism and performance optimization using central composite design and surface modeling. *J. Environ. Manage.* 206, 383–397. <https://doi.org/10.1016/j.jenvman.2017.10.058>.
- Zhai, M. et al, 2017. Gasification characteristics of sawdust char at a high-temperature steam atmosphere. *Energy* 128, 509–518. <https://doi.org/10.1016/j.energy.2017.04.083>.
- Zhang, J., Li, X., Xie, W., Hao, Q., 2018. Handy synthesis of robust Ni/carbon catalysts for methane decomposition by selective gasification of pine sawdust. *Int. J. Hydrogen Energy* 43 (42), 19414–19419. <https://doi.org/10.1016/j.ijhydene.2018.08.207>.
- Zhang, J., Xie, W., Li, X., Hao, Q., Chen, H., Ma, X., 2018. Methane decomposition over Ni/ carbon catalysts prepared by selective gasification of coal char. *Energy Convers. Manage.* 177 (September), 330–338. <https://doi.org/10.1016/j.enconman.2018.09.075>.
- Zhang, J., Jiang, P., Gao, F., Ren, Z., Li, R., Chen, H., 2020. Fuel gas production and char upgrading by catalytic CO₂ gasification of pine sawdust char. *Fuel* 280, (April). <https://doi.org/10.1016/j.fuel.2020.118686> 118686.
- Zhao-qiang, Z., Hong-ying, X., Srinivasakannan, C., Jin-hui, P., 2014. Utilization of Crofton weed for preparation of activated carbon by microwave induced CO₂ activation. *Chem. Eng. Process. Process Intensif.* 82, 1–8. <https://doi.org/10.1016/j.cep.2014.05.001>.
- Zhiwei, C. et al, 2021. Experimental study on gasification of oil sludge with steam and its char characteristic. *J. Hazard. Mater.* <https://doi.org/10.1016/j.jhazmat.2021.125713>.
- Zhong, Y., Zhou, B., Zhang, C., Wu, D., 2018. Effects of surface oxygen functional groups on activated carbon on the adsorption and photocatalytic degradation activities of a TiO₂-AC hybrid for methylene blue and methylene orange. *Carbon N. Y.* 130, 844–845. <https://doi.org/10.1016/j.carbon.2017.10.059>.
- Zhou, Y., Lu, J., Zhou, Y., Liu, Y., 2019. Recent advances for dyes removal using novel adsorbents: a review. *Environ. Pollut.* 252, 352–365. <https://doi.org/10.1016/j.envpol.2019.05.072>.